





RESEARCH ARTICLE

Open Access



Metal contamination in a sediment core from Osaka Bay during the last 400 years

Kai Nils Nitzsche^{1,8*} , Toshihiro Yoshimura¹, Naoto F. Ishikawa¹, Hiroto Kajita^{1,2,3}, Hodaka Kawahata^{3,4}, Nanako O. Ogawa¹ , Katsuhiko Suzuki⁵ , Yusuke Yokoyama^{1,4,6,7} and Naohiko Ohkouchi¹ 

Abstract

Osaka Bay adjacent to the Kyoto–Osaka–Kobe metropolitan area was affected by severe metal pollution during the twentieth century; yet little is known about the trace metal sources and pre-industrial human activities. We have determined the elemental concentrations and zinc stable isotope ratios ($\delta^{66}\text{Zn}$) in bulk sediments and the trace metal concentrations in chemical fractions of a 9-m-long sediment core from Osaka Bay. Our goals were (1) to reconstruct the historical trace metal contamination, and (2) to identify anthropogenic Zn sources and the solid phases of anthropogenic trace metals. The core provided a continuous environmental record of the last 2300 years based on radiocarbon dating of molluscan shells. Copper, Zn, and Pb showed an initial enrichment from the 1670s AD, which could be caused by human activities due to an increasing population. In agreement with previous findings, the trace metal concentrations slightly increased from the 1870s, strongly increased from the beginning of the twentieth century, and peaked around 1960 before environmental pollution control laws were enacted. Increasing trace metal concentrations in the acid-labile and reducible fractions obtained by the Community Bureau of Reference (BCR) sequential extraction procedure toward the surface indicate carbonates and Mn oxyhydroxides were the primary fractions for anthropogenic trace metals. The $\delta^{66}\text{Zn}$ values (1) were constant until the 1940s, suggesting that the average $\delta^{66}\text{Zn}$ of industrial sources was indistinguishable from that value of the natural background, (2) showed a slight decrease from the 1950s and remained constant until the present, and (3) fell in a binary mixing process between a lithogenic ($\sim +0.27\text{‰}$) and an anthropogenic endmember ($\sim +0.17\text{‰}$), the latter likely representing a mixture of various Zn sources such as road dust, tire wear, industrial effluents, and effluents from wastewater treatment plants. We conclude the combination of Zn stable isotopes together with chemical fractions obtained by the BCR method represents a promising approach to assess the trace metal sources and their potential mobility in sediment cores from anthropogenically affected coastal areas.

Keywords: Trace metal, Enrichment factor, Zinc isotope, Osaka Bay, Sediment core, Sequential extraction

1 Introduction

Coastal bays adjacent to large cities are prone to trace metal contamination from various points and diffusive sources originating in their catchments, posing a threat to aquatic life (Barletta et al. 2019; de Souza Machado

et al. 2016). Osaka Bay in the eastern part of the Seto Inland Sea is located directly next to Osaka City, which is part of the Kyoto–Osaka–Kobe metropolitan area, the second largest metropolitan area in Japan. Rapid industrialization and urbanization paired with lacking environmental standards for industrial wastewater, and emissions led to a dramatic increase in the trace metal concentrations from the beginning of the twentieth century (Hosono et al. 2010; Yasuhara and Yamazaki 2005). Yet, little is known about the metal sources, the

*Correspondence: nitzsche@geo.tu-darmstadt.de

¹ Biogeochemistry Research Center, Japan Agency for Marine–Earth Science and Technology (JAMSTEC), 2-15 Natsushima-Cho, Yokosuka, Kanagawa 237-0061, Japan

Full list of author information is available at the end of the article

speciation of trace metals in the sediment, and pre-industrial metal pollution.

Early human activities such as mining, smelting of weapons, and artifacts for worshipping can be trace metal sources. Pre-industrial mining and metallurgy could be traced in lake sediment cores from Europe and the South American Andes (Cooke and Bindler 2015). Zong et al. (2010) suggested smelting of metal tools increased the Cu and Pb concentrations in the sediment of the river mouth of the Pearl River 2000 years ago. Urban activities and the construction of the Great Buddha statue in ancient Nara, Japan, during the eighth century increased the Cu, Hg, and Pb concentrations in adjacent soils (Kawahata et al. 2014). Osaka, formerly known as Naniwa, has a long history dating back to the Kofun period (250–592 AD) and was the scenery of repeated warfare during the Sengoku period (1467–1615 AD) (see Sect. 2.3); thus, human activities such as smelting presenting could be expected as potential metal sources.

Trace metals deposited into the aquatic environment are present in different solid phases in the sediment. The trace metals in these phases can be extracted using the Community Bureau of Reference (BCR) sequential extraction procedure (Rauret et al. 1999), which provides insights into their bioavailability, potential mobility, and transferability. Yasuhara and Yamazaki (2005) suggested metal pollution strongly contributed to the decline in ostracode absolute abundance in a core close to the Yodo River mouth at the inner part of the bay from the early 1910s to the 1970s AD. Similarly, metal pollution was believed to have contributed to the decline in marine organisms at other sites in the Seto Inland Sea (Irizuki et al. 2018). Thus, trace metal chemical fractions could provide insights into potential toxicological effects on marine biota. Recently, Tonhá et al. (2020) showed the combination of the trace metals extracted by the BCR method with zinc stable isotopes ($\delta^{66}\text{Zn}$) was a promising tool to trace Zn contamination and redistribution in sediments from coastal Sepetiba Bay, Brazil.

Industrial processes such as redox reactions, evaporation (e.g., during smelting, and coal combustion), and dissolution (e.g., in wastewater treatment plants) cause a significant Zn isotopic fractionation (c.f. Desaulty and Petelet-Giraud 2020). Often, the $\delta^{66}\text{Zn}$ values of the resulting Zn (by)products differ from that of the Upper Continental Crust (UCC; $+0.28 \pm 0.05$ ‰, 2σ) (Chen et al. 2013). Typical contemporary anthropogenic materials with low $\delta^{66}\text{Zn}$ values are road dust ($+0.08$ ‰ to $+0.17$ ‰) and tire wear ($+0.08$ ‰ to $+0.21$ ‰) (Dong et al. 2017; Souto-Oliveira et al. 2018; Thapalia et al. 2010), and industrial waters and effluents from wastewater treatment plants (-0.03 ‰ to $+0.15$ ‰) (Chen et al. 2008; Desaulty and Petelet-Giraud 2020; Sakata et al.

2019). Anthropogenic materials with high $\delta^{66}\text{Zn}$ values are slags and effluents from smelters (up to $+1.5$ ‰) (Juillot et al. 2011; Sivry et al. 2008) and Zn in electroplating wastes after electrochemical reduction (up to $+3.5$ ‰) (Kavner et al. 2008). As such, combining $\delta^{66}\text{Zn}$ values with changes in Zn concentrations has become a popular tool for tracing anthropogenic Zn in sediment cores from coastal areas throughout the Anthropocene time (Araújo et al. 2017, 2019a; b; Sakata et al. 2019; Tonhá et al. 2020).

In this study, we have investigated the temporal variations in the weathering intensities, and the trace metal concentrations in bulk sediments and chemical fractions and Zn stable isotope ratios in a 9-m-long sediment core from Osaka Bay. Owing to the long history of Osaka (Naniwa), we aimed for reconstructing the historical trace metal contamination. In addition, we compare the historical trace metal contamination with sediment cores from other sites in the Seto Inland Sea, and we assess potential toxic effects on marine biota. Sakata et al. (2019) suggested the contribution of Zn discharged from electroplating plants led to increasing $\delta^{66}\text{Zn}$ values in a core from Tokyo Bay from the early 1950s. Such a pattern may also exist for Osaka Bay. Thus, our second goal was to identify the anthropogenic Zn sources and the solid phases of anthropogenic trace metals. We show that the combination of Zn stable isotopes with trace metal chemical fractions obtained by the BCR method represents a powerful tool to study the anthropogenic Zn sources and their potential bioavailability.

2 Study area and materials

2.1 Osaka Bay and its catchment

Osaka Bay is located at the eastern end of the Seto Inland Sea in southwestern Japan (Additional file 1: Fig. S1). The bay covers approximately 1500 km² and has a mean depth of approximately 30 m and is partly enclosed by the Awaji Island in the West. The whole catchment of the bay covers a total area of approximately 10,700 km² and it consists of several subbasins. The Yodo River in the Osaka plain is the primary freshwater source with an annual estimated discharge of 5.14 km³ year⁻¹ and a catchment area of 8240 km² including the catchment area of Lake Biwa (3170 km²). Minor rivers are the Yamato River (0.43 km³ year⁻¹, 1070 km²), the Muko River (496 km²), and the Ina River (383 km²). In addition, numeral smaller rivers with steep gradients have their origins in Mount Rokkō northeast of the lowlands near Kobe City and in the Kongō Range in the South.

The geology of the whole catchment is complex consisting mainly of Quaternary unconsolidated sediments of alluvial plain and terrace deposits primarily of fluvio-lacustrine origin (Itihara et al. 1988), and clastic (meta)sedimentary rocks of the Jurassic and Cretaceous

accretionary complexes (Fig. 1). Cretaceous granitoid rocks are mostly exposed in the eastern part of the catchment. Felsic volcanic and volcanoclastic rocks mostly occur in the northwest and in the southeast. Gneisses and schists of the Ryoke Belt, Carboniferous to Permian limestones and basalts, and Cretaceous gabbros are mostly present in the eastern part.

Large cities in the direct vicinity are Osaka, Kobe, Sakai, Nishinomiya, and Amagasaki, while Kyoto is located further northeast. Consequently, large urban and build-up land areas are present in the catchment (Fig. 1).

2.2 Sediment sampling

A piston core and a multiple core were collected at station OS5B from the central part of Osaka Bay (34° 31.632 N, 135° 12.606 E) at a water depth of 24 m during cruise KT-11-13 on July 1, 2011 (Additional file 1: Fig. S1). The piston core consists of gray homogenous muddy sediments with no distinguishable substantial changes in the sedimentary facies as shown by observations of the continuous section of the core using X-ray computed tomography (CT). The core was carefully cut in 2 cm slices from the surface to the final core depth of 884 cm. The multiple core was 33 cm long and was cut into 1 cm slices.

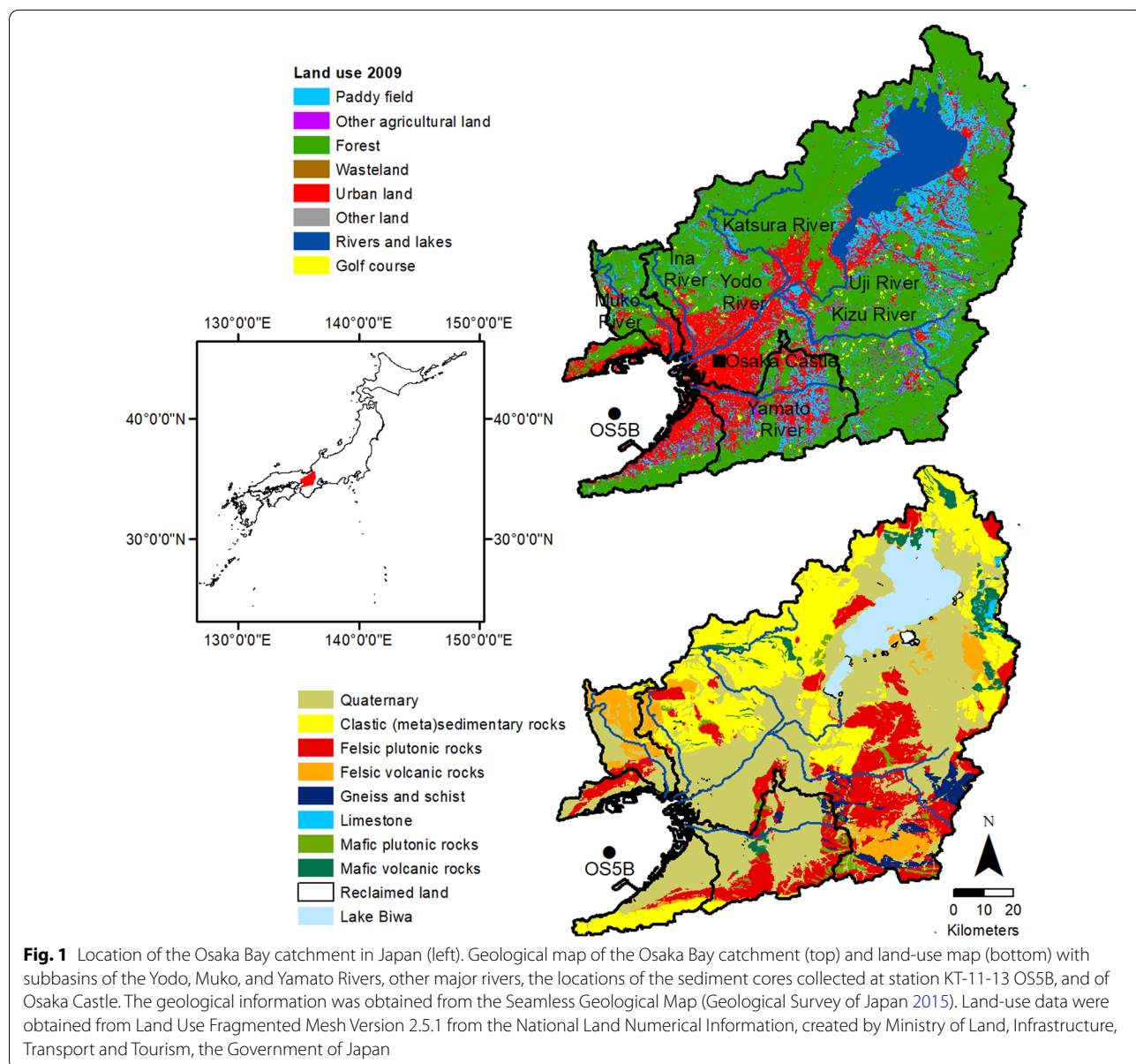


Fig. 1 Location of the Osaka Bay catchment in Japan (left). Geological map of the Osaka Bay catchment (top) and land-use map (bottom) with subbasins of the Yodo, Muko, and Yamato Rivers, other major rivers, the locations of the sediment cores collected at station KT-11-13 OS5B, and of Osaka Castle. The geological information was obtained from the Seamless Geological Map (Geological Survey of Japan 2015). Land-use data were obtained from Land Use Fragmented Mesh Version 2.5.1 from the National Land Numerical Information, created by Ministry of Land, Infrastructure, Transport and Tourism, the Government of Japan

2.3 Historical events in the catchment

In the following, we summarize major transformations of the Osaka Bay catchment and human activities that have potentially affected the sedimentation rates, the sediment sources, the weathering intensities, and the trace metal input into the bay.

2.3.1 Yayoi period (ca. 930 BC to 250 AD)

The sea level changes and the evolution of Osaka Bay were firstly summarized by Kajiyama and Itihara (1972). In the present study, we refer to more recent data on the evolution of Osaka Bay (Matsuda 2008). During the Yayoi period, large parts of the present Osaka city were underwater (Fig. 2). Osaka Bay reached further east to the Uemachi Plateau, a peninsula connected to the landmass in the South. The brackish Kawachi Lagoon was located between the Uemachi Plateau in the West and the Ikoma mountain range in the East. The Yodo River in the North-east and the Yamato River (formerly called Nagase River) in the Southeast emptied into the bay creating alluvial fans. Eventually, due to a growing sand bar north of the Uemachi Plateau, Kawachi Lagoon turned into a freshwater lake from 400 BC to around 1 BC. From as early as 700 BC, rice cultivation started leading to permanent habitation on the Uemachi Plateau and around the Kawachi plain (c.f. Pearson 2016).

2.3.2 Transition (Kofun) period (ca. 250 to 592 AD)

During the fifth century AD, a canal, Naniwa no Horie, was dug through the sandbar which connected the sea with Kawachi Lake (Fig. 2). A port facility, called Naniwa-tsu, with large warehouses was constructed at the tip of the Uemachi Plateau, which allowed for trade with the Chinese mainland and with the Korean peninsula, promoting the growth of the city. Furthermore, huge Mozu tombs (Kofun) were constructed.

2.3.3 Imperial and aristocracy period (592 to 1185 AD)

Owing to the increasing sedimentation and propagation of the Yodo and Yamato Rivers by the beginning of the Heian period (from 794 AD), the original Kawachi Lake had largely disappeared and turned into a fertile marshland (Kawachi plain) with smaller lakes and numerous rivers suitable for rice cultivation. Naniwa-tsu continued to grow as an urban center including the digging of canals and rice irrigation. However, from the ninth century AD Naniwa lost its importance for trade.

2.3.4 Feudal period (1183 to 1868 AD)

During the Kamakura (1183–1333) and Muromachi periods (1336–1573), the development of rice fields continued. From 1570 to 1580, Ishiyama Hongan-ji, an important temple constructed in 1496, was besieged

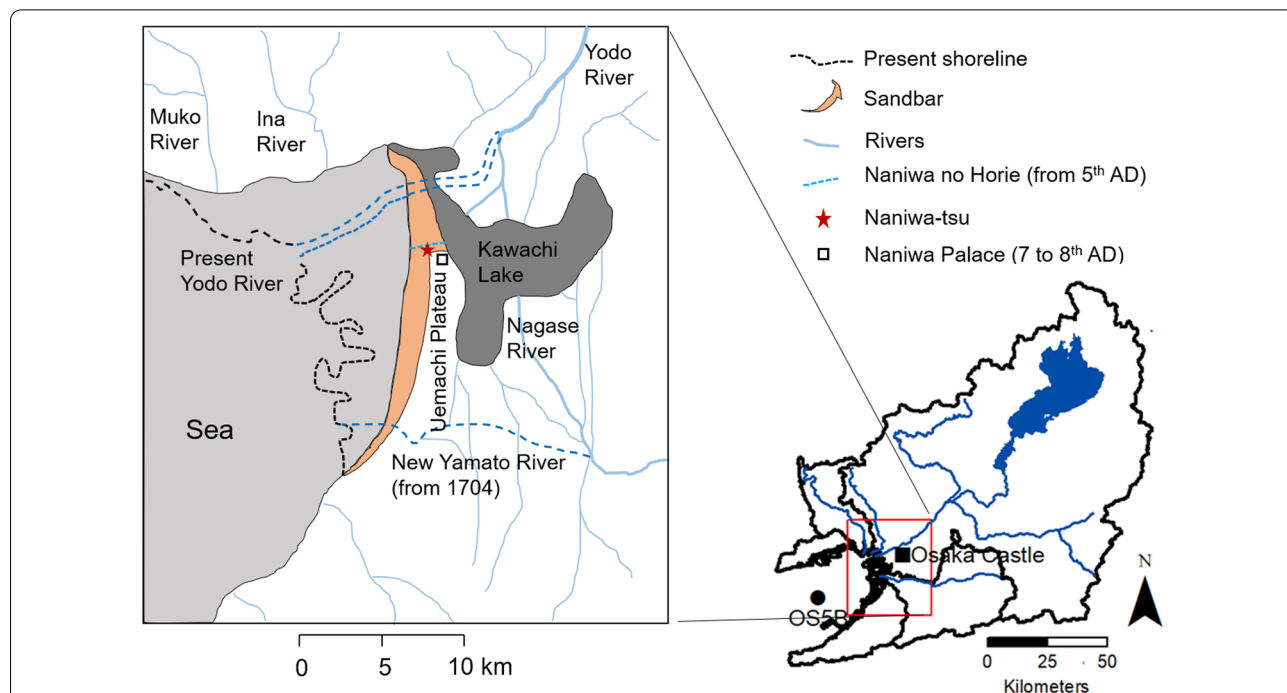


Fig. 2 Kawachi Lake during the third and fourth centuries AD with location of the inset in the Osaka Bay catchment. The locations of the Naniwa no Horie canal, the port Naniwa-tsu (constructed in the fifth century AD), of Naniwa Palace, and of the present Yodo River and Yamato River are also shown. Modified after Kajiyama and Itihara (1986), Kajiyama and Itihara (1972), and Kusaka (2012)

by Nobunaga Oda. In 1583, the construction of Osaka Castle began, which was completed in 1597 by Hideyoshi Toyotomi on the grounds of the former Ishiyama Hongan-ji. Several flood control measures around Osaka Castle, Yodo River, and its tributaries, were initiated by Hideyoshi Toyotomi. Following the destruction of Osaka Castle in 1615 at the beginning of the Edo period (1603–1868), Osaka became an important economic hub. In 1704, the rerouting of the Yamato River into Osaka Bay was completed (Fig. 2). As a consequence, the Kawachi plain (the current Osaka plain) was spared from flooding, leading to the formation of new arable land for rice and cotton cultivation.

2.3.5 Modern period (1868 AD to present)

During the early Meiji era, large parts of the Osaka plain were still used for rice cultivation (Additional file 1: Fig. S2), but most agricultural lands disappeared during the following decades. Following the opening of the Osaka harbor in 1868, the Modern period began, and the industrialization was initiated. Rapid industrialization, urbanization, and population growth took place from about 1890 (the start of Japan's industrial revolution) and during Japan's post-war period of economic growth (1955–1973). Furthermore, the Osaka metropolitan area was heavily bombed in 1945.

3 Material and methods

3.1 Core dating

Twenty-seven molluscan shells were selected from the piston core for age dating. They were dated via radiocarbon measurement by accelerator mass spectrometry (AMS) at the Micro Analysis Laboratory of the University of Tokyo (Matsuzaki et al. 2004; Yokoyama et al. 2019). The employed technique for sample preparation was reported previously (Yokoyama et al. 2007), yet described briefly as follows. After ultrasonic cleaning, approximately 15 mg of shell samples was weighed, and weak acid was added to remove secondary CaCO_3 (>15% of outer shell weight). After vacuum drying overnight, the cleaned sample was converted to CO_2 with phosphoric acid under vacuum conditions. The product CO_2 was passed through a vacuum line and target graphite was formed on iron powder in a hydrogen atmosphere heated at 650 °C. The graphite was pressed into target holders and analyzed via AMS.

All radiocarbon age results were calibrated to calendar years using the OxCal ver. 4.4 software (Bronk Ramsey 2009) with the Marine 20 dataset (Heaton et al. 2020). A regional-specific reservoir (DR) correction of 135 ± 20 years was used, which was estimated for Beppu Bay, located in the Seto Inland Sea, by Kuwae et al. (2013).

3.2 Total organic carbon and total nitrogen analysis

The total organic carbon (TOC) and total nitrogen (TN) concentrations were determined from 0 to 40 cm core depth of piston core ($n=20$), and for each cm until 19 cm and then for every second cm until 33 cm core depth of the multiple core ($n=26$), respectively. With respect to the multiple core, the TOC concentrations were determined after weighing approximately 20 mg of powdered sample into a silver capsule, decalcification with 1 M HCl, and drying at 80 °C, using a Flash 2000 CHNS elemental analyzer at the Geological Survey of Japan, Tsukuba (National Institute of Advanced Science and Technology). The TN concentrations were determined on the unacidified samples. For the piston core, the TOC and TN concentrations were determined after weighing samples into pre-cleaned smoothed wall tin capsules, decalcification with 0.5 M HCl, and drying on a hotplate at 80 °C. The tin capsules with the dried samples were sealed and analyzed by a sensitivity-improved elemental analyzer (Flash EA1112, Thermo Finnigan, Bremen, Germany) connected to an isotope ratio spectrometer (Delta plus XP, Thermo Finnigan, Bremen, Germany) at the Biogeochemistry Research Center, JAMSTEC, according to Ogawa et al. (2010).

3.3 Grain size analysis

The mean grain size of 100 selected horizons of the piston core was analyzed on a Mastersizer 2000 laser diffraction particle size analyzer (Malvern Panalytical, UK) at Kochi Core Center, JAMSTEC. The wet sediment samples were pretreated with 1.2 M HCl and 2 M Na_2CO_3 to remove carbonates and biogenic opal, respectively. After checking under the microscope for any remaining biological source particles, the samples were dispersed with 0.01 M $(\text{NaPO}_3)_6$.

3.4 Digestion of the bulk sediment

For chemical analyses of the piston core, subsamples of each horizon (without the surface sediment from 0 to 2 cm) were taken until 132 cm core depth, every 10 cm until 482 cm, and every 50 cm until 878 cm. The subsamples were freeze-dried, and the <125 μm fraction was manually dry-sieved and powdered. The powdered bulk sediment samples were digested with HNO_3 –HF– HClO_4 similar to the protocol described in Yokoyama et al. (1999). The samples were evaporated to dryness and re-dissolved in 1 M HNO_3 for further analysis.

3.5 Sequential extraction

We determined the distribution of trace metals in the acid-soluble (F1), reducible (F2), oxidizable (F3), and residual (F4) fractions of 56 samples using a modification of the revised Community Bureau of Reference

(BCR) method (Table 1) (Rauret et al. 1999; Sahuquillo et al. 1999). In the current study, single extractions were performed using a 100 mg sample while maintaining the same sample/solution ratios, the supernatant was removed by pipetting, and the residue was washed three times with methanol and evaporated to dryness at 60 °C. To ensure the complete reaction of the acid-soluble fraction with acetic acid, step F1 was repeated as we observed a decline in the pH value after the first F1 extraction indicating that carbonates were still present. To account for exchangeable metals, ten samples covering a wide range in bulk Cu, Zn, and Pb concentrations were extracted with 1 M NH₄Cl and shaken for 3 h. Replicate extraction ($n=4$) of the Tokyo Bay sediment JMS-1 standard yielded an uncertainty of typically <5% (1σ) for Cu, Zn, Pb, Co, and Ni.

3.6 Chemical and isotopic analyses

Aliquots of digested bulk sediments and of chemical fractions were analyzed for elemental concentrations (Co, Ni, Cu, Zn, Pb, Na, K, Ca, Al, Fe, Ti, Mn, Ba, Sr) using a quadrupole inductively coupled plasma mass spectrometry (iCAP Q ICP-MS; Thermo Scientific, Bremen, Germany) at JAMSTEC. The analytical precision (1σ) based on replicate analysis of the JMS-1 standard during the measurements was typically <3%.

Zinc was purified from solutions that contained 2.4 μ g Zn with the BioRad anion-exchange resin AG1-X8 (200–400 mesh) in Cl form using a modified version of the protocol described in Sossi et al. (2015). Briefly, Zn was eluted with 2 mL of Milli-Q water after washing the resin with 5 mL of 8 M HCl, 5 mL of 3 M HCl, and 4 mL of 0.4 M HCl. To ensure Zn solutions were free of any matrix elements (e.g., Al, Ti), the separation was repeated one more time. The final Zn extract was evaporated to dryness, re-dissolved in 0.5 mL HNO₃ and 0.05 mL H₂O₂ and heated at 140 °C to digest organics from the resin, again evaporated to dryness, and finally re-dissolved in 2% HNO₃. The Zn recovery was $99 \pm 6\%$ based on the Zn concentrations analysis of the Zn solutions.

The Zn concentration in the purified samples was adjusted to 300 ppb. The Zn stable isotope ratios were measured on these solutions under wet plasma

conditions with low-resolution mode using a Neptune Plus Multicollector ICP-MS (Thermo Scientific, Bremen, Germany) at the Submarine Resources Center, JAMSTEC. The samples were analyzed using the standard-sample-standard bracketing method with the newly developed AA-ETH standard (Archer et al. 2017). Specifically, three separate analyses of the same sample solution were conducted, for which uncertainties were reported as two standard deviations (2σ). The instrumental mass fractionation was corrected using Cu-doping (Maréchal et al. 1999) after adjusting the Cu/Zn ratios to 1:1 in the sample solutions. To allow for comparison with the previously published literature, the ⁶⁶Zn/⁶⁴Zn ratios are expressed in delta notation relative to the JMC-LYON standard according to the following Eq. (1):

$$\delta^{66}\text{Zn}_{\text{JMC-LYON}} = \left(\frac{(^{66}\text{Zn}/^{64}\text{Zn})_{\text{sample}}}{(^{66}\text{Zn}/^{64}\text{Zn})_{\text{AA-ETH}}} \right) \cdot 1000 + 0.28 \quad (1)$$

An error propagation associated with the conversion of $\delta^{66}\text{Zn}_{\text{AA-ETH}}$ to $\delta^{66}\text{Zn}_{\text{JMC-LYON}}$ was not performed as the analytical uncertainty was usually greater than the error related to the conversion. The quality control of the $\delta^{66}\text{Zn}$ values was assured by analyzing the NIST 682 high-purity Zn standard. The repeated measurement of NIST 682 yielded a $\delta^{66}\text{Zn}$ value of $-2.42 \pm 0.04 \text{ ‰}$ ($n=12$, 2σ), which corresponds to values reported elsewhere (Conway et al. 2013; John et al. 2007). Furthermore, the accuracy of the measurements was assessed by analyzing the reference sediments Jlk-1 (Lake Biwa), JMS-1 (Tokyo Bay), and MESS-4 (Beaufort Sea, Arctic Canada), which underwent the same purification protocol as the samples. The repeated measurement of Jlk-1 yielded a $\delta^{66}\text{Zn}$ value of $+0.27 \pm 0.03 \text{ ‰}$ ($n=11$) and that of JMS-1 was $+0.29 \pm 0.04 \text{ ‰}$ ($n=10$). The $\delta^{66}\text{Zn}$ value of MESS-4 was $+0.26 \pm 0.05 \text{ ‰}$ ($n=8$), which agreed well with a previously reported value of $+0.26 \pm 0.02 \text{ ‰}$ ($n=4$, 2σ) (Jeong et al. 2021).

3.7 Enrichment factor and chemical alteration index

The enrichment factor (EF) of the trace metals was calculated as an index for the anthropogenic contamination

Table 1 Overview of the sequential extraction procedure with nominal target phases

Step	Fraction	Nominal target phases	Extractant
1	Acid soluble	Soluble and exchangeable species, carbonates	0.11 M acetic acid (repeated)
2	Reducible	Fe and Mn oxyhydroxides	0.5 M hydroxylamine hydrochloride, pH = 1.5
3	Oxidizable	Organic matter and sulfides	8.8 M hydrogen peroxide followed by 1 M ammonium acetate, pH = 2
4	Residual	Silicates and well-crystalline oxides	Nitric acid, hydrofluoric acid, perchloric acid

and to account for textural differences across the samples (Andrews and Sutherland 2004; Chen et al. 2007). For this purpose, the concentration of a trace metal of interest (M) is normalized to the concentration of a conservative element according to Eq. (2):

$$EF_M = \frac{\left(\frac{M}{Al}\right)_{\text{sample}}}{\left(\frac{M}{Al}\right)_{\text{UCC}}} \quad (2)$$

Aluminum was chosen as the conservative element because Al is widespread in aluminosilicate minerals and relatively immobile during most weathering regimes. The concentration ratio of the sample (M/Al_{sample}) was then normalized to that ratio in the Upper Continental Crust (M/Al_{UCC}) using the following elemental concentrations of the UCC reported by Rudnick and Gao (2014): Al $81,497 \mu\text{g g}^{-1}$, Zn $67 \mu\text{g g}^{-1}$, Cu $28 \mu\text{g g}^{-1}$, Pb $17 \mu\text{g g}^{-1}$, Co $17.3 \mu\text{g g}^{-1}$, and Ni $47 \mu\text{g g}^{-1}$. The EF was interpreted according to Chen et al. (2007): $EF < 1$: no enrichment, $EF < 3$ minor enrichment, $EF = 3-5$ moderate enrichment, $EF = 5-10$ moderately severe enrichment, $EF = 10-25$ severe enrichment, $EF = 25-50$ very severe enrichment, and $EF > 50$ extremely severe enrichment.

The chemical index of alteration (CIA) of the residual fraction (F4) was calculated as a measure of the degree of weathering that rocks have experienced (Nesbitt and Young 1982) according to Eq. (3):

$$CIA = \left(\frac{Al_2O_3}{Al_2O_3 + CaO + Na_2O + K_2O} \cdot 100 \right) \% \quad (3)$$

The CIA usually ranges from about 50 for fresh rocks comprising “primary minerals” to around 100 for completely weathered rocks comprising secondary clay minerals (Young and Nesbitt 1998).

3.8 Statistical analyses

The Pearson product–moment correlation analysis was used to explore relationships between the Zn concentrations and the Zn stable isotope ratios. We explored relationships between the metal concentrations of the compositional (closed) bulk elemental data by performing a Spearman product–moment correlation analysis of symmetric coordinates that were obtained after an isometric log-ratio (ilr) transformation of the data. Using symmetric coordinates for correlation analysis provides a better representation of the relationship between two variables than classical correlation analysis between two pairs of variables as the latter neglects the influence of all other variables (Garrett et al. 2017; Kynčlová et al. 2017; Reimann et al. 2017). The statistical analyses were performed using R (version 4.1.2, R

Foundation for Statistical Computing, Vienna, Austria, <http://www.R-project.org/>). Spearman correlation coefficients were computed for the symmetric coordinates of the data using the function “`gx.symm.coords.r`” from the R package “`rgr`” (Garrett 2018). The Spearman correlation coefficients were visualized in a heatmap with different colors for positive and negative correlations after arranging the columns and rows using hierarchical clustering (average linkage using Euclidean distances) with distances based on the correlations as suggested by Reimann et al. (2017). This allows for visualizing clusters of positive and negative correlations, respectively. The heatmap was drawn with the function “`heatmap.2`” from the package “`gplots`.”

4 Results

4.1 Age model

The age model for the piston core was constructed using a P-sequence deposition model (Bronk Ramsey 2008; Bronk Ramsey and Lee 2013), which was implemented in the computer program OxCal. In constructing the age model, we excluded five ^{14}C age values based on relatively poorly preserved shell samples and the ^{14}C value that exceeded 1950 AD when calibrated (Table 2). The boundary of the change in the sediment accretion rate (SAR) was set to a core depth of 310 cm because the slope between the uncalibrated ^{14}C age and the core depth was changing, and the mean grain size showed a slight decrease from 270 cm ($65 \pm 7 \mu\text{m}$, average \pm standard deviation, $n=31$) compared to greater depths ($73 \pm 8 \mu\text{m}$, $n=70$) (Fig. 3). The drop in the SAR could be caused by changes in the coastal currents (Yasuhara et al. 2002).

The piston core provided a continuous environmental record of the last 2300 years as shown by the calendar age–depth profile (Fig. 3). The calibrated age of a shell at 16 cm depth exceeded 1950 AD indicating that this sample was affected by the radiocarbon bomb pulse peaked in 1963 AD in the Northern Hemisphere when the Partial Test Ban Treaty took effect. To account for a possible loss of the upper part of the piston core, we compared the TOC and TN concentrations between the piston core and the multiple core (Additional file 1: Fig. S3). TOC and TN showed a slight offset between the piston core and the multiple core of around 8 cm indicating that approximately the top 8 cm of the piston core were lost during the sampling. Assuming that the age of the surface layer of the multiple core is 2011 AD, we interpolated the age of the horizons from 0 to 33 cm of the piston core revealing that 0 cm core depth corresponded to approximately 1997 AD.

Table 2 Depth and radiocarbon-derived dates ($\pm 1\sigma$) of the molluscan shells retrieved from the piston core. The range of calendar ages defines a 68.2% confidence interval

Sample type	Lab. code	Depth (cm)	Conventional ^{14}C age (year BP)	Calibrated age (unmodeled) (Cal. year BP)	Calibrated age (modeled) (Cal. year BP)	Comment
Snail	MTC-15894	16	-627 ± 41	Out of calibration	Out of calibration	a
Mollusca	MTC-16218	34	496 ± 63	49 ± 40	21 ± 23	
Bivalve	MTC-16219	68	898 ± 64	217 ± 99	136 ± 29	
Mollusca	MTC-16220	70	399 ± 52	40 ± 30	143 ± 30	
Mollusca	MTC-16221	100	887 ± 66	207 ± 99	265 ± 30	
Mollusca	MTC-16222	148	1282 ± 68	567 ± 76	466 ± 31	
Bivalve	MTC-15951	152	857 ± 58	178 ± 91	–	b
Mollusca	MTC-15896	178	1287 ± 52	570 ± 66	582 ± 31	
Snail	MTC-16223	212	1576 ± 65	826 ± 89	714 ± 32	
Bivalve	MTC-15897	222	1442 ± 52	703 ± 78	751 ± 33	
Echinus	MTC-15952	310	1816 ± 62	1075 ± 93	1090 ± 44	
Echinus	MTC-16224	336	2145 ± 65	1413 ± 93	–	b
Echinus	MTC-15899	338	1946 ± 57	1201 ± 85	1148 ± 41	
Echinus	MTC-16225	378	1915 ± 70	1169 ± 95	1230 ± 38	
Mollusca	MTC-16226	459	2370 ± 65	1660 ± 105	–	b
Echinus	MTC-15953	481	2164 ± 59	1431 ± 89	1444 ± 32	
Bivalve	MTC-15901	541	2285 ± 54	1561 ± 95	1569 ± 31	
Mollusca	MTC-15954	571	2379 ± 75	1672 ± 114	1632 ± 32	
Mollusca	MTC-16228	599	2615 ± 65	1959 ± 112	–	b
Bivalve	MTC-15902	623	2448 ± 52	1753 ± 96	1740 ± 34	
Echinus	MTC-16230	677	2518 ± 71	1840 ± 114	1852 ± 38	
Mollusca	MTC-16231	689	2455 ± 73	1763 ± 114	1877 ± 39	
Bivalve	MTC-15955	691	2785 ± 72	2169 ± 116	–	b
Mollusca	MTC-15903	777	2687 ± 56	2051 ± 106	2064 ± 49	
Echinus	MTC-16232	807	2810 ± 72	2198 ± 116	2128 ± 53	
Echinus	MTC-15904	839	2818 ± 55	2207 ± 99	2195 ± 58	

a: Excluded from the calculation of the sedimentation age model using P-sequence because the calibrated age exceeded 1950 AD

b: Excluded from the calculation of the sedimentation age model using P-sequence because the analyzed shells are of poor preservation

4.2 Trace metal concentrations and enrichment factors of the bulk sediment, and chemical index of alteration

The Cu, Zn, Pb, Co, and Ni concentrations remained relatively constant from the bottom of the core (~ 300 BC) until the 1670s AD (Fig. 4), from when the Cu, Zn, and Pb concentrations showed a slight increase (Fig. 5). The Cu concentrations further increased until approximately 1800 AD. From the mid-1870s, Zn, Cu, Pb, and Co showed a slight increase until the mid-1930s, from when a rapid increase was observed until approximately 1960 AD. The trace metal concentrations then declined until the mid-1970s from when they remained constant until approximately 1990 AD. In contrast, Ni showed a substantial increase from the early 1910s until the early 1940s AD, from when a rapid decrease was observed.

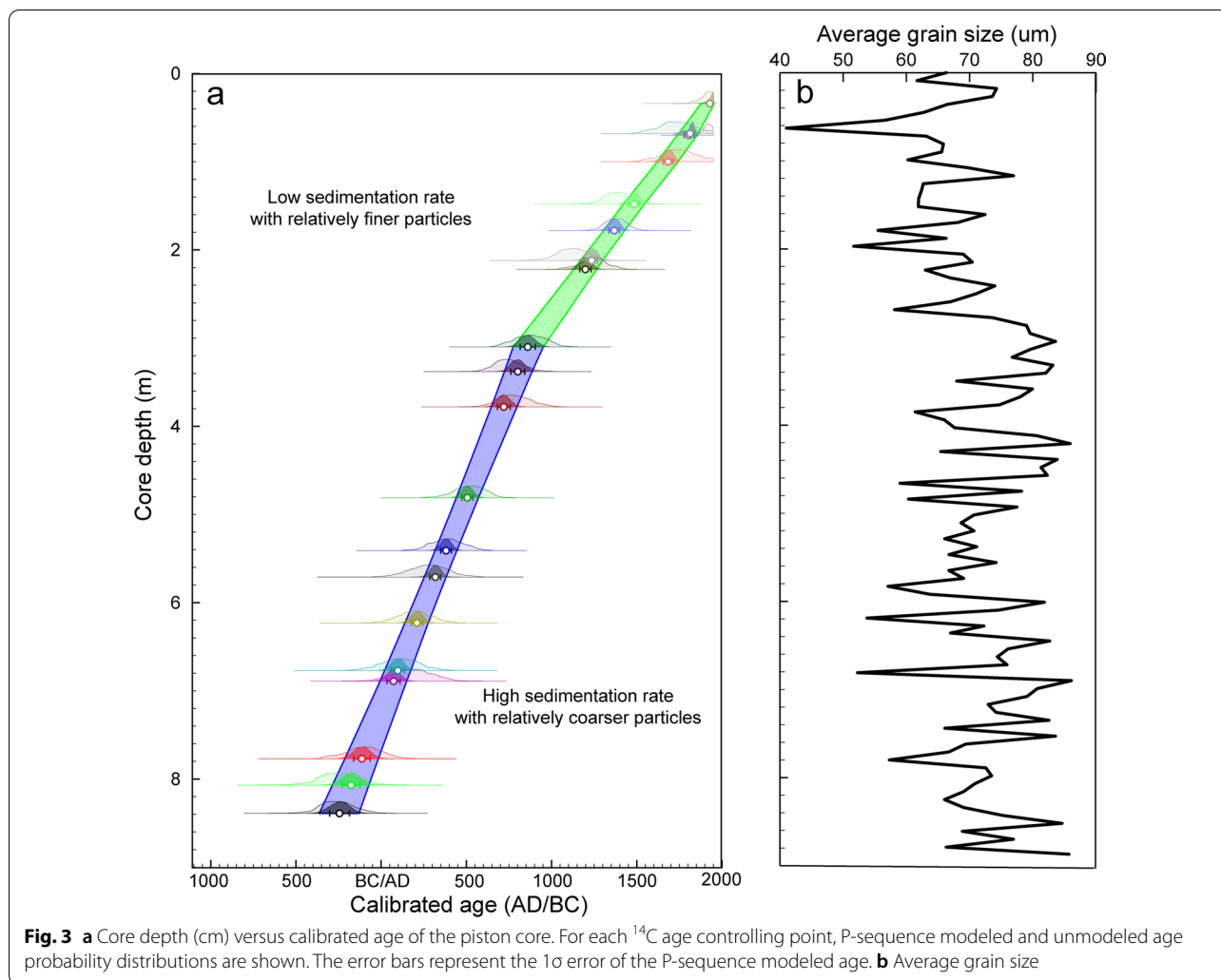
Nickel and Co usually showed no enrichment ($EF < 1$), Cu and Pb showed a minor enrichment ($EF < 3$), and Zn showed a moderate enrichment ($EF < 5$) (Fig. 6 and

Additional file 1: Fig. S4). The temporal trends of the enrichment factors generally agree with those of the trace metal concentrations. The heatmap of correlation coefficients based on the symmetric coordinates showed a cluster of Mn, Pb, Cu, and Zn (Fig. 7).

The CIA showed only mineral variation throughout the whole core (75–78%) (Additional file 1: Fig. S5).

4.3 Trace metals concentrations in the chemical fractions

The temporal trends of the Cu, Zn, and Co concentrations in the acid-labile, reducible, and oxidizable fractions generally agreed with those in the bulk sediments, i.e., Cu and Zn showed an initial increase from the 1670s AD, a slight increase from the mid-1870s and a strong increase from the mid-1930s peaking around 1950 (Fig. 8). In case of Pb, the reducible fraction reflected the temporal trend of the bulk sediments. For Ni, a rapid increase was observed for the residual fraction from the early 1910s,



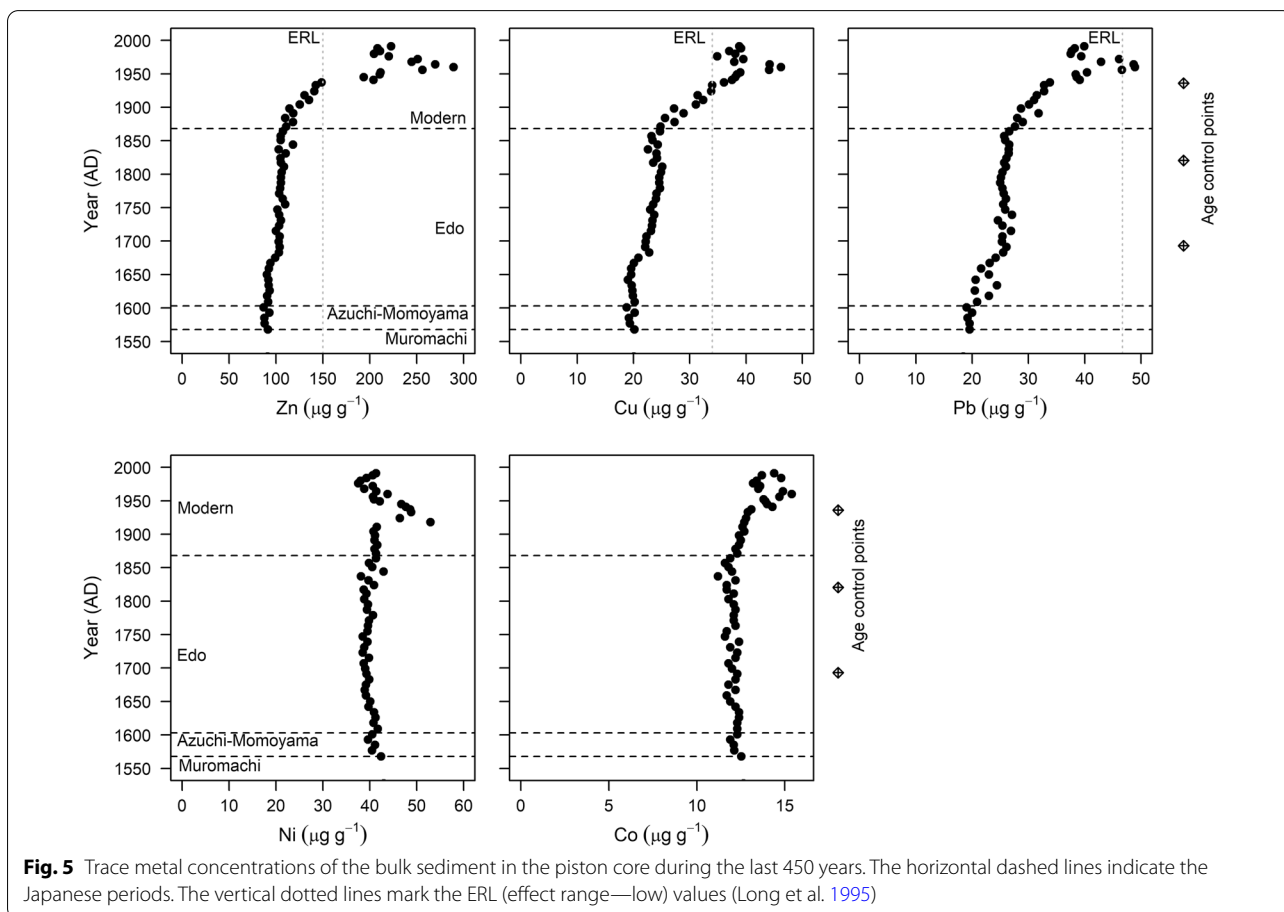
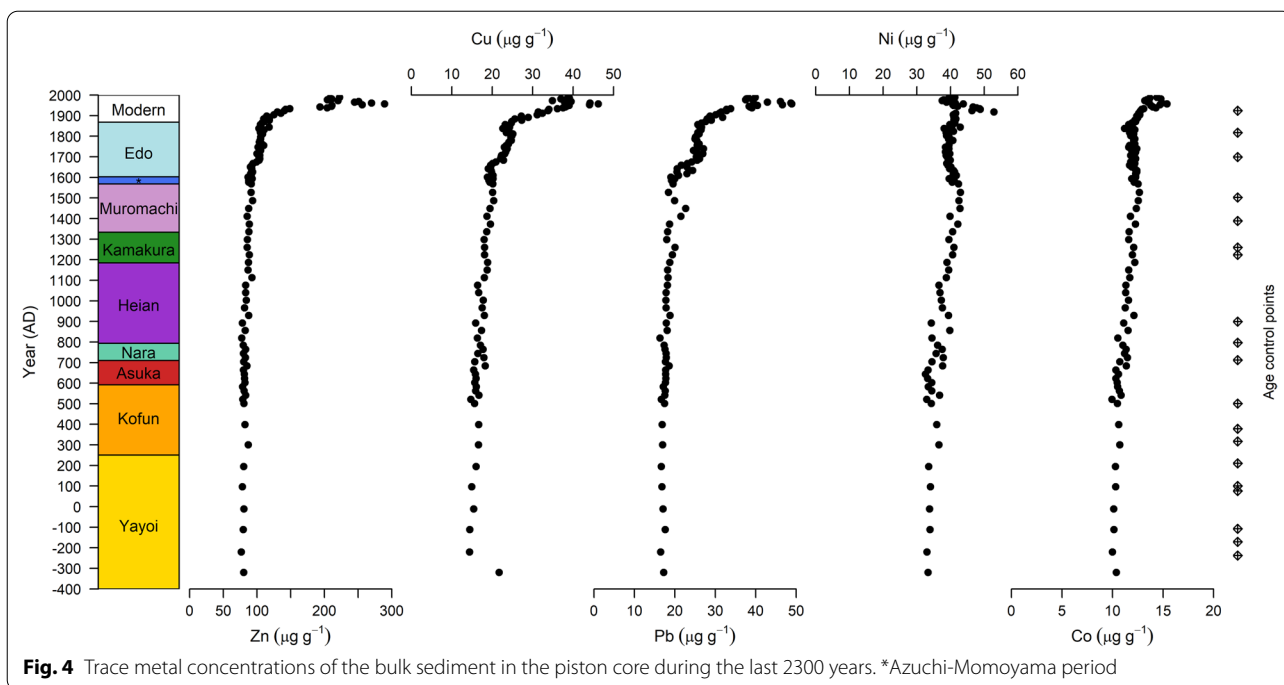
decreasing from the early 1940s, while the other fractions showed only marginal changes.

Owing to the temporal trends in the chemical fractions, the proportion of trace metals in the different fractions has changed across the core (Fig. 9). Zinc was usually hosted in the residual fraction (31–79%), followed by the acid-labile (3–35%), the reducible (8–26%) and the oxidizable fraction (9–12%). Copper was mainly hosted in the residual fraction (40–73%), followed by the oxidizable (17–26%), the reducible (6–26%), and the acid-labile (1–11%) fractions. Cobalt primarily occurred in the residual fraction (52–64%), followed by the acid-labile (11–24%), reducible (10–16%), and oxidizable (8–12%) fractions. In contrast, most Pb occurred in the reducible (usually 52–75%, followed by the residual (17–47%) fractions, while only little Pb was present in the acid-soluble (1–8%) and oxidizable (0.3–3%) fractions. Nickel was typically found in the residual fraction (74–86%). Furthermore, Cu in the exchangeable fraction accounted for

up to 55% in the acid-soluble fraction, Zn represented up to 18%, Ni and Pb usually up to 10%, and Co up to 2% for the ten samples tested (Additional file 1: Table S1). The proportion of exchangeable Cu was on average 1.5 and that of Zn 3.0 times higher, respectively, in the five pre-1890 samples without anthropogenic contamination.

4.4 Zinc stable isotopes

The $\delta^{66}\text{Zn}$ values of the bulk sediment were relatively constant until the early 1940s with on average $+0.27 \pm 0.01\text{‰}$ ($n=15$, 2σ) (Fig. 6, Additional file 1: Table S2). The $\delta^{66}\text{Zn}$ values then showed an abrupt decrease to on average $+0.22 \pm 0.01\text{‰}$ ($n=13$), which was constant until around 1990. The $\delta^{66}\text{Zn}$ values were negatively correlated with EF_{Zn} ($r=-0.79$, $P<0.01$; Fig. 10a) and with the logarithm of the sum in Zn concentrations of the acid-soluble and the reducible fractions ($r=-0.83$, $P<0.01$).



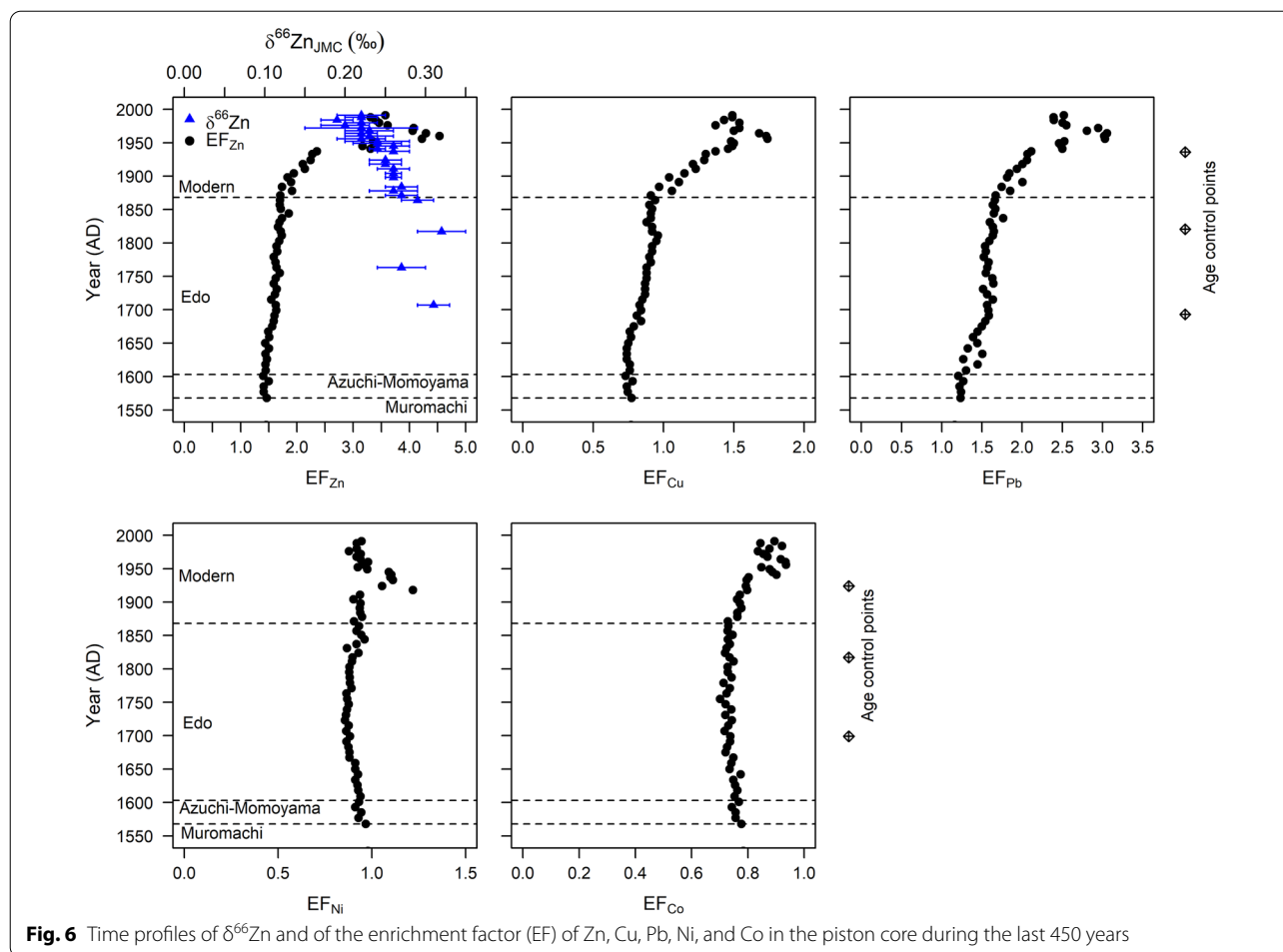


Fig. 6 Time profiles of $\delta^{66}\text{Zn}$ and of the enrichment factor (EF) of Zn, Cu, Pb, Ni, and Co in the piston core during the last 450 years

5 Discussion

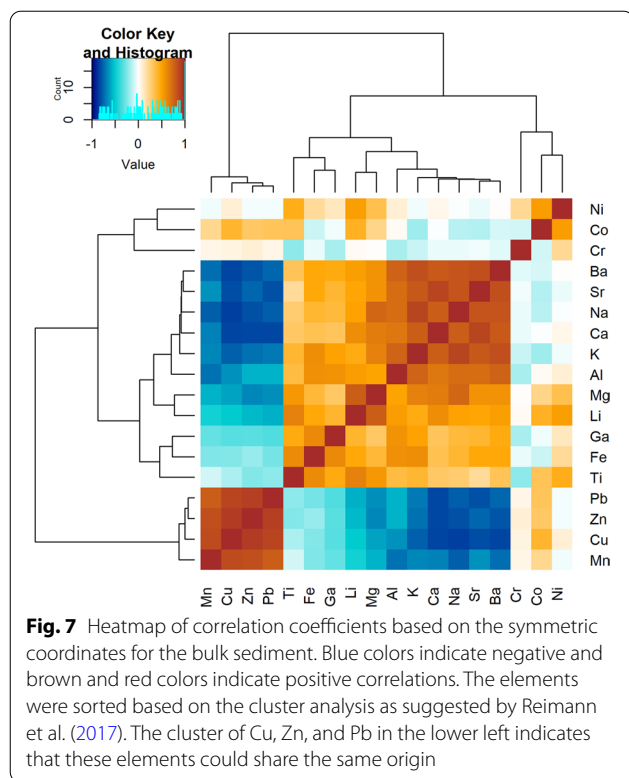
5.1 Trace metals before the Edo period

The relatively constant trace metal concentrations and enrichment factors before the Edo period (Fig. 4 and Additional file 1: Fig. S4) indicate that early human activities were negligible trace metal sources. Although there was a constant inhabitation of the Osaka area with rice cultivation during the Yayoi and Kofun periods, smelting was not much known yet, and many metal tools were likely imported from the Korean peninsula (Rhee et al. 2007). Iron smelting (*tatara*) for metal tools, weapons, and armor was performed from the end of the fifth century (Pearson 2016), but did not affect the trace metal concentrations, and neither did the warfare during the Sengoku period (1467–1615 AD).

5.2 Metal pollution during the Edo period

The increase in the Zn, Cu, and Pb concentrations from the 1670s AD (Figs. 5, 8) is later than the reconstruction of Osaka Castle (1620–1629 AD) after its destruction in 1615 AD by the Tokugawa forces. Thus, it is possible

that human activities owing to an increasing population in the Osaka area at the beginning of the peaceful Edo period led to a trace metal input into the bay. The relatively constant Zn and Pb concentrations until the 1870s agree with the stable population in the Osaka area during the Edo period (Saito 2002). The increasing Cu concentrations until the beginning of the early nineteenth century AD could be caused by emissions from ore smelting by the Sumitomo Copper Refinery established about 1 km southwest of Osaka Castle in 1655 AD and expanded in 1690 AD, which processed copper from the Besshi Copper Mines, Ehime Prefecture, from 1690 AD (Suzuki et al. 1998). Although significant correlations between the trace metal concentrations and the CIA exist (Additional file 1: Fig. S6), it is unlikely that slightly enhanced weathering intensities caused the trace metal enrichment from the 1670s AD and the 1870s AD. Instead, human activities have likely affected the weathering intensities due to deforestation and rice cultivation, while the trace metal enrichment was due to anthropogenic metal inputs.



5.3 Metal pollution during the modern age

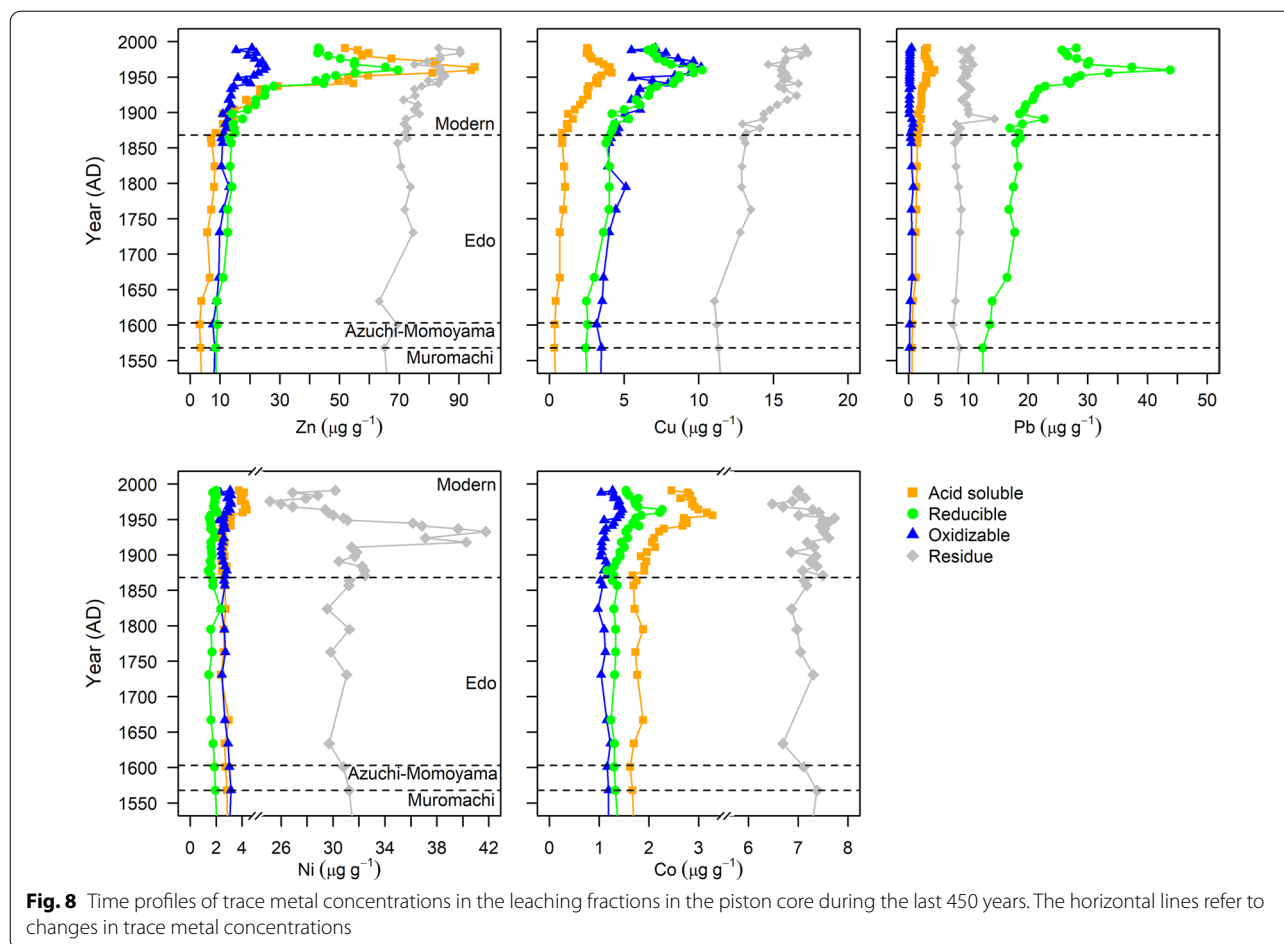
The gradual increase in the Zn, Cu, Pb, and Co concentrations in the bulk sediments (Fig. 5) and leachate fractions (Fig. 8) from the 1870s also observed for the inner bay (Yasuhara and Yamazaki 2005) marks the beginning of early industrialization in the Osaka area. The second half of the nineteenth century AD in Japan was characterized by the industrial revolution and urbanization promoted by the Meiji government (from 1868 AD). The industrialization in the Osaka area included coal combustion, ore smelting, shipbuilding, cotton spinning, and others. For instance, several Cu smelters started operating at the end of the nineteenth century AD. Furthermore, the population of Osaka City increased rapidly from the end of the nineteenth century AD (Fig. 11). The rapid increase in the Zn and Pb concentrations from the 1930s agrees with those previously found in a sediment core from the inner bay (Yasuhara and Yamazaki 2005) and cores from the central bay (Hosono et al. 2010), and falls within the period of economic growth following the Japanese-Russo War (1904–1905 AD) and World War I (1914–1918 AD). Furthermore, the recovery stage (1946–1954 AD) and the period of rapid economic growth (1955–1973 AD) led to increasing trace metal emissions. Due to the enactment of environmental pollution laws during the late 1960s and 1970s AD, the trace metal concentrations have been decreasing. In the present study, the peaks in the trace

metal concentrations around 1960 agree well with those observed for other sediment cores in Osaka Bay (Hosono et al. 2010; Yasuhara and Yamazaki 2005) and for the Osaka Castle moat (Inano et al. 2004).

In comparison with other sediment cores from the Seto Inland Sea, metal pollution in Osaka Bay started earlier (1870s AD) than Harima-Nada (from around 1900 AD) (Hoshika et al. 1983), Hiroshima Bay (from the 1930s AD) (Yasuhara et al. 2003), Beppu Bay (from the early 1920s AD) (Irizuki et al. 2022), and than Hiuchi-nada (from the 1950s AD) (Irizuki et al. 2018). This is not surprising because the Osaka area was rapidly industrialized following the opening of its port. However, the trace metal pollutions typically peaked during the 1960s for all sites in the Seto Inland Sea due to the legal restrictions on wastewater and remain still high at present indicating that attempts to reduce trace metal pollution are not enough and that the redistribution of legacy metals is still problematic.

The cluster of correlations between Mn, Pb, Cu, and Zn (Fig. 7) indicates a similar origin of Cu, Zn, and Pb, as well as a strong association with Mn phases. Trace metal containing smelter and other industrial effluents were directly transferred into rivers, which discharge into the bay. Furthermore, Zn, Cu, and Pb released into the atmosphere by coal combustion and ore processing have entered the aquatic domain by atmospheric deposition. Fe–Mn oxyhydroxides formed in the water column could scavenge these trace metals, while up to 55% of Cu and 18% of Zn within the acid-soluble fraction, respectively (Additional file 1: Table S2), were weakly adsorbed onto clay surfaces such as of kaolinite and smectite. Calcifying organisms such as foraminifers incorporate Zn and a small amount of Cu into their shells and into their biomass indicated by the increasing trace metal concentrations in the acid-labile and oxidizable fractions from the 1870s (Figs. 8, 9). For instance, some benthic foraminifera incorporate more Zn with increasing Zn concentrations in the ambient seawater (Smith et al. 2020). Furthermore, organic matter degradation and the reductive dissolution of Fe–Mn oxyhydroxides in subsurface sediments release initially bound trace metals into the porewater, which can subsequently re-adsorb to carbonates, clay minerals, and sulfides (Canavan et al. 2007; Dang et al. 2015). In our previous study on a sediment core from nearby Lake Biwa, we also found that the acid-labile and reducible fractions were the main hosts of anthropogenic trace metals (Nitzsche et al. 2021) highlighting the role of Mn oxyhydroxides for trace metal association in sediment cores from freshwater and coastal environments.

Not only are the trace metal concentrations higher during the 1980s than in pre-industrial times albeit the discharge restrictions from the 1970s (Fig. 5), but they are



also in more bioavailable and mobile fractions (Fig. 8) with possible toxic effects to marine biota. Potential toxicological effects on marine organisms can be assessed based on the ERL (effect range—low) and ERM (effect range—medium) values of the sediment guidelines of the US Environmental Protection Agency (USEPA) (Long et al. 1995). The ERL values for Cu, Zn, and Pb are 34, 150, and 46.7 $\mu\text{g g}^{-1}$, and the ERM values are 270, 410, and 218 $\mu\text{g g}^{-1}$, respectively. Thus, the Cu concentrations slightly exceeded the ERL value from the 1930s until the 2000s, while Pb only exceeded the ERL around 1960 (Fig. 5). Zinc started to exceed the ERL value from the early 1950s but remained below the ERM value. Thus, metal pollution exceeding the ERL values in these periods could have affected Osaka Bay's marine organisms and ecosystem negatively. More toxic effects were observed in the inner bay (Yasuhara et al. 2007; Yasuhara and Yamazaki 2005).

5.4 Zinc stable isotopes as tracer for Zn contamination

In this study, we have used Zn stable isotope ratios to assess anthropogenic Zn sources. Because the anthropogenic Zn

was primarily associated with carbonates and with Fe–Mn oxyhydroxides in the sediment core (Figs. 8, 9), Zn isotopic fractionation during the adsorption onto mineral surfaces must be considered (Komárek et al. 2022). Zinc adsorbed on calcite is isotopically heavy (Dong and Wasylenki 2016) and the heavy Zn isotopes are preferentially incorporated into calcite (Mavromatis et al. 2019). Similarly, the adsorption onto Fe–Mn oxyhydroxides favors the heavy isotopes (Balistrieri et al. 2008; Bryan et al. 2015; Juillot et al. 2008). Thus, it is likely that the decreasing $\delta^{66}\text{Zn}$ values toward the surface were due to changes in metal sources rather than isotopic fractionation during complexation with surfaces. Future studies will have to determine the $\delta^{66}\text{Zn}$ values in the trace metal chemical fractions to test why the detected isotopic fractionation during adsorption found in laboratory studies does not affect $\delta^{66}\text{Zn}$ values in the bulk sediments.

Although a doubling of EF_{Zn} from the 1870s until the 1940s was observed, the relatively constant $\delta^{66}\text{Zn}$ values ($+0.27 \pm 0.01\%$) (Fig. 6) indicated that the average $\delta^{66}\text{Zn}$ value of the anthropogenic Zn overlapped with that of the UCC ($+0.28 \pm 0.05\%$, 2σ) (Chen et al. 2013). For

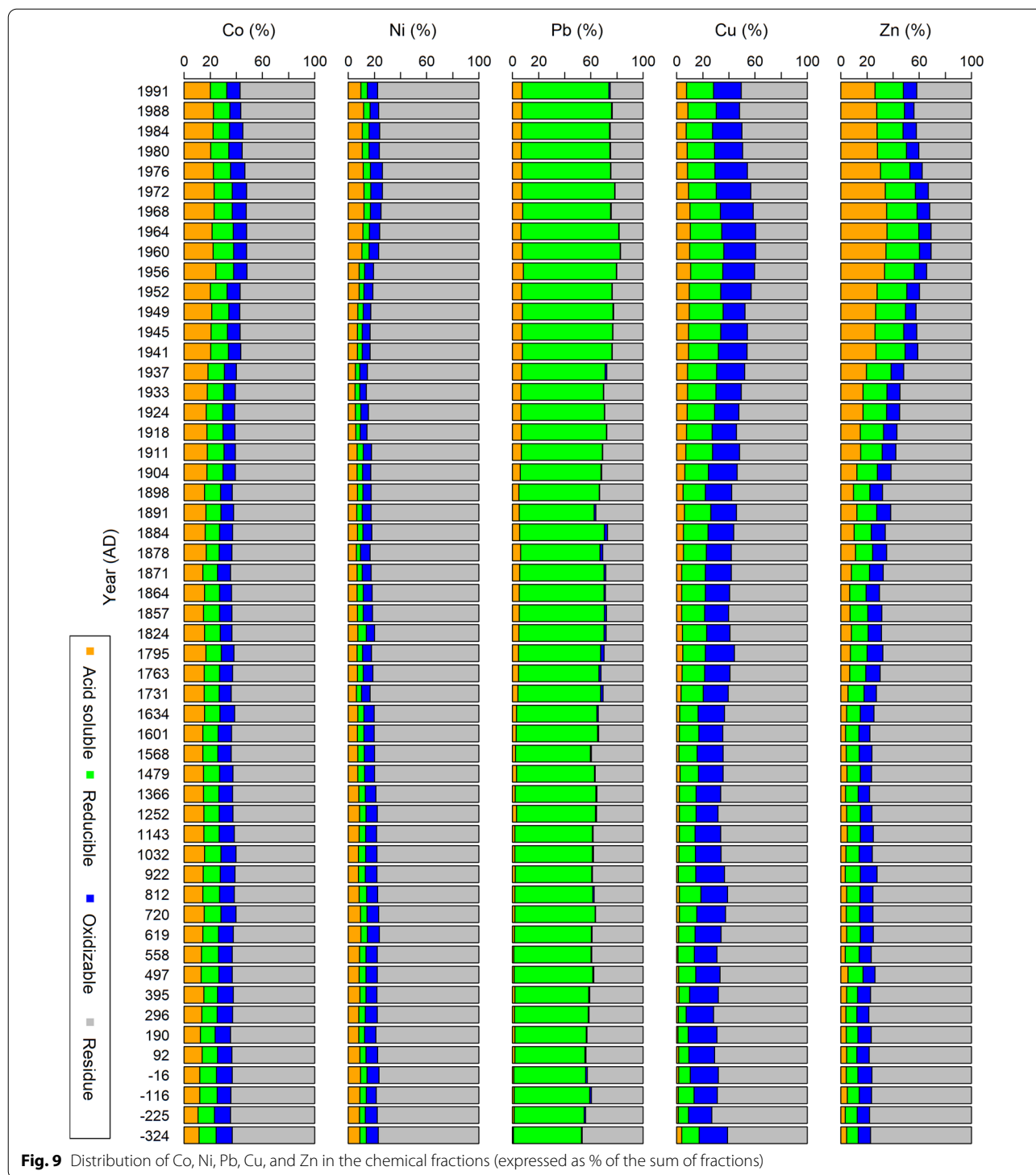
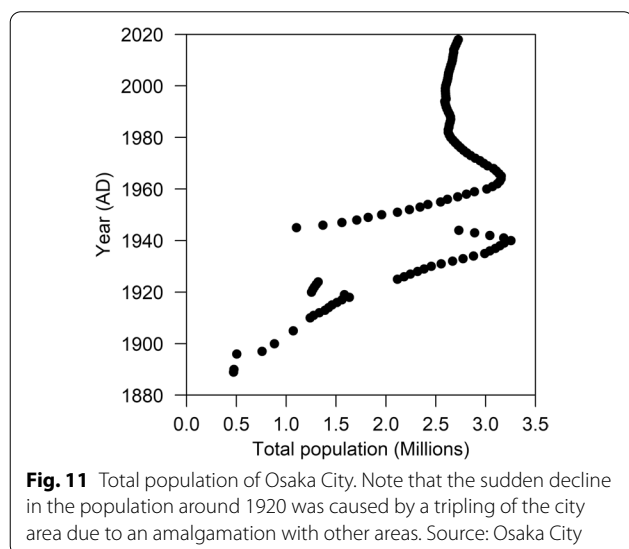
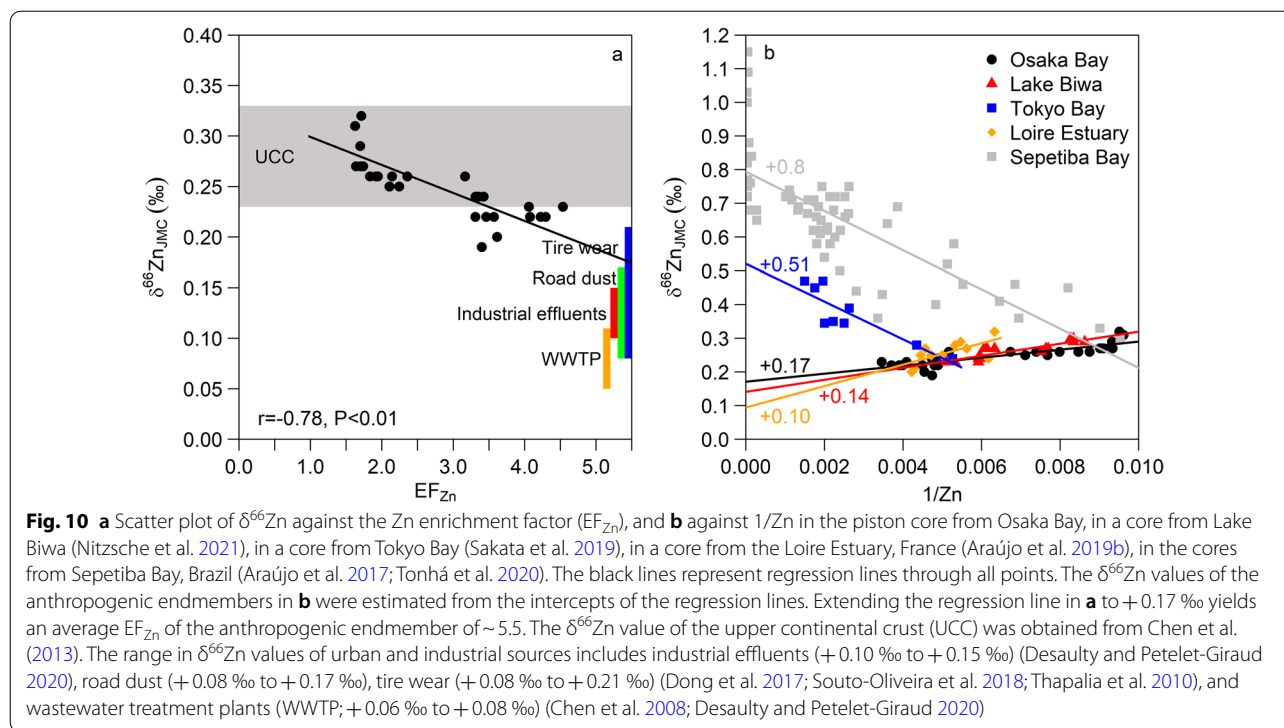


Fig. 9 Distribution of Co, Ni, Pb, Cu, and Zn in the chemical fractions (expressed as % of the sum of fractions)

instance, the estimated $\delta^{66}\text{Zn}$ values of fly ash particles from coal combustion span a wide range from -0.31 to $+1.26\text{‰}$ depending on the $\delta^{66}\text{Zn}$ of the coal (Desaulty and Petelet-Giraud 2020; Ochoa Gonzalez and Weiss

2015). Particles emitted by Zn smelters tend to have low $\delta^{66}\text{Zn}$ values ($-0.39 \pm 0.05\text{‰}$), while slags and water leaching the slag tailings tend to be enriched in ^{66}Zn ($+0.51$ to 1.18‰) (Desaulty and Petelet-Giraud 2020).



The abrupt decrease to on average $+0.22 \pm 0.01$ ‰ from the early 1950s indicates the enhanced contribution of a ^{66}Zn -depleted source. Such a decrease was also observed for Lake Biwa from the late 1950s (Nitzsche et al. 2021). The negative correlation between $\delta^{66}\text{Zn}$ and EF_{Zn} ($r = -0.79$, $P < 0.01$; Fig. 10a) indicates a binary mixing between a natural endmember ($+0.27$ ‰) and urban anthropogenic sources with

lower $\delta^{66}\text{Zn}$ values as previously suggested for urban lakes across the US (Thapalia et al. 2015, 2010) and the Loire estuary, France (Araújo et al. 2019b). We have estimated the average $\delta^{66}\text{Zn}$ value of the anthropogenic endmember as $+0.17 \pm 0.01$ ‰ based on the intercept of the regression line between $\delta^{66}\text{Zn}$ and $1/\text{Zn}$ (Fig. 10b). This value was close to the value observed for Lake Biwa $+0.14 \pm 0.02$ ‰ (Nitzsche et al. 2021) and slightly higher than the ranges of urban and industrial sources observed in other studies. Typical anthropogenic sources with low $\delta^{66}\text{Zn}$ values include industrial effluents (hospitals, chemical industries, agro-food industry, surface treatment industry; $+0.10$ ‰ to $+0.15$ ‰) (Desaulty and Petelet-Giraud 2020), road dust ($+0.08$ ‰ to $+0.17$ ‰), tire wear ($+0.08$ ‰ to $+0.21$ ‰). Other sources such as gasoline (-0.50 ‰ to -0.23 ‰) (Dong et al. 2017; Gioia et al. 2008; Souto-Oliveira et al. 2019; Thapalia et al. 2010) and atmospheric industrial emissions (-0.60 ‰ to $+0.15$ ‰) (Ochoa Gonzalez et al. 2016; Souto-Oliveira et al. 2018) could be of minor importance as they are more depleted in ^{66}Zn . Low $\delta^{66}\text{Zn}$ values in rainwater in the Uji area, south of Lake Biwa, were attributed to road dust and Zn emitted via high-temperature processes such as smelters and fire power plants (Takano et al. 2021).

Using the $\delta^{66}\text{Zn}$ value of the anthropogenic endmember (+0.17‰), we can estimate the anthropogenic Zn contribution in a simple binary mixing model (Araújo et al. 2021) according to Eq. (4):

$$\text{Zn}_{\text{anthropogenic}} = \frac{\delta^{66}\text{Zn}_{\text{sample}} - \delta^{66}\text{Zn}_{\text{natural}}}{\delta^{66}\text{Zn}_{\text{natural}} - \delta^{66}\text{Zn}_{\text{anthropogenic}}} \quad (4)$$

In this equation, $\delta^{66}\text{Zn}_{\text{sample}}$ corresponds to the $\delta^{66}\text{Zn}$ value of a sample, $\delta^{66}\text{Zn}_{\text{natural}}$ is the $\delta^{66}\text{Zn}$ value of the natural endmember (+0.27‰), and $\delta^{66}\text{Zn}_{\text{anthropogenic}}$ represents the $\delta^{66}\text{Zn}$ value of the anthropogenic endmember (+0.17‰). We found the contribution of the anthropogenic endmember increased from approximately 10% in the mid-1940s up to 80% around 1980 (Additional file 1: Fig. S7).

Furthermore, the reduction in untreated domestic wastewater (+0.28 ± 0.02‰, $n=1$, Chen et al. 2008) and of industrial effluents, and the contribution of water from wastewater treatment plants (WWTPs; +0.05‰ to +0.11‰) (Chen et al. 2008; Desaulty and Petelet-Giraud 2020; Sakata et al. 2019) from the early 1970s did not have a significant effect on the $\delta^{66}\text{Zn}$ values until around 1990. The constant $\delta^{66}\text{Zn}$ values could be due to similar $\delta^{66}\text{Zn}$ values of anthropogenic sources and/or the contribution of contaminated river sediments and runoff from industrial and urban areas (Andronikov et al. 2021). In contrast to the positive relationship between $\delta^{66}\text{Zn}$ and 1/Zn observed for Osaka Bay, a negative relationship was observed for a core from Tokyo Bay owing to increasing $\delta^{66}\text{Zn}$ values from the 1950s until +0.47‰ in the early 1970s (Sakata et al. 2019). Sakata et al. (2019) estimated a $\delta^{66}\text{Zn}$ value of +0.51‰ for the anthropogenic endmember, and the authors suggested the contribution of Zn discharged from electroplating plants, which started to operate in the early 1950s. Similarly, Araújo et al. (2017) suggested the $\delta^{66}\text{Zn}$ value of the major anthropogenic Zn source associated with electroplating wastes was +0.86 ± 0.15‰ in Sepetiba Bay, Brazil. Tonhá et al. (2020) showed that the anthropogenic Zn was mainly hosted in the acid-soluble fraction in Sepetiba Bay. Similarly, we found a negative correlation between the $\delta^{66}\text{Zn}$ values with the logarithm of the sum of the Zn concentrations of the acid-soluble and the reducible fractions ($r = -0.83$, $P < 0.01$) implying that the anthropogenic Zn was hosted in these two bioavailable and mobile fractions. Today, there are 302 electroplating companies in Tokyo prefecture and 195 companies in Osaka prefecture with a smaller number of companies in neighboring prefectures that are part of Tokyo and Osaka Bays, respectively (Japan Federation of Electro Plating Industry Association 2003). Thus, it is likely that effluents

from electroplating plants enriched in ^{66}Zn were also discharged into Osaka Bay to some extent, but quantification remains difficult. Consequently, albeit the Tokyo and the Osaka metropolitan areas are the two largest metropolitan areas in Japan, which suffered from severe metal pollution during the twentieth century, the Zn stable isotope data reveal that the Zn sources differed based on the industries in the catchment.

6 Conclusions

This study showed the temporal variation of trace metals and Zn stable isotopes in a sediment core from Osaka Bay during the last 2300 years. The BCR sequential extraction procedure showed that carbonates and Mn oxyhydroxides were the primary hosts for anthropogenic trace metals in the core. An initial trace metal enrichment from the 1670s indicated pre-industrial activities. Although a doubling of EF_{Zn} from the 1870s until the mid-1940s AD was observed, the constant $\delta^{66}\text{Zn}$ values showed that the early anthropogenic Zn sources (e.g., coal combustion) were indistinguishable from the natural background highlighting the limitation of Zn stable isotopes as tracers for early industrialization. Instead, more contemporary Zn sources depleted in ^{66}Zn (e.g., road dust, tire wear, industrial effluents, effluents from WWTPs) (Desaulty and Petelet-Giraud 2020) caused a decrease in the $\delta^{66}\text{Zn}$ values from the early 1950s and throughout the later twentieth century. This decrease is opposite to the increasing $\delta^{66}\text{Zn}$ values observed for Tokyo Bay from the 1950s suspected due to effluents from electroplating companies enriched in ^{66}Zn (Sakata et al. 2019). Consequently, Zn stable isotopes allow tracing different anthropogenic Zn sources in bays adjacent to metropolitan areas, while the BCR method can provide further insights into the potential mobility of Zn and other trace metals.

Abbreviations

AD: Anno Domini; AMS: Accelerator mass spectrometry; BC: Before Christ; BCR: Community Bureau of Reference; BP: Before present; CIA: Chemical index of alteration; CT: X-ray computed tomography; $\delta^{66}\text{Zn}$: Zinc stable isotope ratio; EF: Enrichment factor; ERL: Effect range—low; ERM: Effect range—medium; JAMSTEC: Japan Agency for Marine-Earth Science and Technology; SAR: Sediment accretion rate; TOC: Total organic carbon; TN: Total nitrogen; UCC: Upper Continental Crust; WWTP: Wastewater treatment plant.

Supplementary Information

The online version contains supplementary material available at <https://doi.org/10.1186/s40645-022-00517-z>.

Additional file 1: Table S1. Cu, Zn, Pb, Co, and Ni concentrations in the exchangeable fraction extracted by 1M NH₄Cl and their proportion (%) in the acid-soluble fraction extracted two times with 0.11M acetic acid (Hac) of ten selected samples. **Table S2.** Bulk Cu, Zn, Pb, Co, and Ni concentrations and $\delta^{66}\text{Zn}$ values of samples analyzed for Zn stable isotopes of the

core OS5B. *ND: not determined. **Fig. S1.** Catchment of Osaka Bay (bold black line) with prefectural boundaries (thin black lines) and location of the sediment cores collected at station OS5B. **Fig. S2.** Swampy lowlands during the early Meiji era. Source: Technical Report of the Geospatial Information Authority of Japan (Technical Report D1-No.633, Marsh data in the early Meiji Era (Kinki District)). **Fig. S3.** Comparison of total organic carbon (TOC) and total nitrogen (TN) concentrations between the piston core and the multi core. **Fig. S4.** Time profiles of the enrichment factor (EF) of Zn, Cu, Pb, Ni, and Co in the piston core during the last 2300 years. *Azuchi-Momoyama period. **Fig. S5.** Time profiles of the chemical index of alteration (CIA) calculated from the residual fraction (F4). *Azuchi-Momoyama period. **Fig. S6.** Biplots of trace metal concentrations against chemical index of alteration (CIA) calculated from the residual fraction (F4). **Fig. S7.** Time profiles of the Zn contribution estimated based on a simple binary mixing model following equation (3).

Acknowledgements

We thank Ami Togami (AORI), Yosuke Miyairi (AORI), Masafumi Murayama (Kochi Core Center), Hiroyuki Matsuzaki (MALT), and the onboard scientists of the KT-11-13 cruise for their support in core drilling, slicing, grain size, and radiocarbon analysis, and Y. Yoshikawa and N. Kudo (both JAMSTEC) for their support in chemical analysis.

Author contributions

KNN, HKawahata, and TY designed the study. KNN carried out the experimental work, analyzed the data, and wrote the first manuscript draft. HKawahata organized the sampling of the sediment core and provided the sediment samples. YY conducted the radiocarbon analysis. HKajita contributed to stratigraphical and chronological interpretations. KNN, TY, and KS conducted the metal concentration and zinc isotope analysis. NOO conducted the TOC and TN analysis of the piston core. KNN and NFI did the literature research. All authors were involved in the data interpretation and edited and approved the final manuscript.

Funding

K. N. Nitzsche was supported by the JAMSTEC Young Research Fellowship. The analytical work was partly supported by JSPS KAKENHI Grant Number 20H00193 to YY.

Availability of data and materials

The research data are available from the corresponding author upon request.

Declarations

Competing interests

The authors declare that they have no competing interests.

Author details

¹Biogeochemistry Research Center, Japan Agency for Marine–Earth Science and Technology (JAMSTEC), 2-15 Natsushima-Cho, Yokosuka, Kanagawa 237-0061, Japan. ²Graduate School of Science and Technology, Hirosaki University, 3, Bunkyo-Cho, Hirosaki, Aomori 036-8561, Japan. ³National Institute of Advanced Industrial Science and Technology, 1-1-1 Higashi, Tsukuba, Ibaraki 305-8567, Japan. ⁴Atmosphere and Ocean Research Institute, The University of Tokyo, 5-1-5 Kashiwanoha, Kashiwa, Chiba 277-8564, Japan. ⁵Submarine Resources Research Center, Japan Agency for Marine–Earth Science and Technology (JAMSTEC), 2-15 Natsushima-Cho, Yokosuka, Kanagawa 237-0061, Japan. ⁶Department of Earth and Planetary Science, Graduate School of Science, The University of Tokyo, 7-3-1 Hongo, Bunkyo-Ku, Tokyo 113-0033, Japan. ⁷Research School of Physics, The Australian National University, Canberra, ACT 2601, Australia. ⁸Present Address: Department of Soil Mineralogy and Soil Chemistry, Institute of Applied Geosciences, Technical University of Darmstadt, Schnittspahnstraße 9, 64287 Darmstadt, Germany.

Received: 30 May 2022 Accepted: 15 October 2022

Published online: 29 October 2022

References

- Andrews S, Sutherland RA (2004) Cu, Pb and Zn contamination in Nuuanu watershed, Oahu, Hawaii. *Sci Total Environ* 324:173–182. <https://doi.org/10.1016/j.scitotenv.2003.10.032>
- Andronikov AV, Novak M, Oulehle F, Chrastny V, Sebek O, Andronikova IE, Stepanova M, Sjpikova A, Hruska J, Myska O, Chuman T, Veselovsky F, Curik J, Prechov E, Komarek A (2021) Catchment runoff in industrial areas exports legacy pollutant zinc from the topsoil rather than geogenic Zn. *Environ Sci Technol* 55:8035–8044. <https://doi.org/10.1021/acs.est.1c01167>
- Araújo DF, Boaventura GR, Machado W, Viers J, Weiss D, Patchineelam SR, Ruiz I, Rodrigues APC, Babinski M, Dantas E (2017) Tracing of anthropogenic zinc sources in coastal environments using stable isotope composition. *Chem Geol* 449:226–235. <https://doi.org/10.1016/j.chemgeo.2016.12.004>
- Araújo DF, Ponzevera E, Briant N, Knoery J, Bruzac S, Sireau T, Brach-Papa C (2019a) Copper, zinc and lead isotope signatures of sediments from a mediterranean coastal bay impacted by naval activities and urban sources. *Appl Geochem* 111:104440. <https://doi.org/10.1016/j.apgeochem.2019.104440>
- Araújo DF, Ponzevera E, Briant N, Knoery J, Sireau T, Mojtahid M, Metzger E, Brach-Papa C (2019b) Assessment of the metal contamination evolution in the Loire estuary using Cu and Zn stable isotopes and geochemical data in sediments. *Mar Pollut Bull* 143:12–23. <https://doi.org/10.1016/j.marpolbul.2019.04.034>
- Araújo DF, Ponzevera E, Weiss DJ, Knoery J, Briant N, Yepez S, Bruzac S, Sireau T, Brach-Papa C (2021) Application of Zn isotope compositions in oysters to monitor and quantify anthropogenic Zn bioaccumulation in marine environments over four decades: a “Mussel Watch Program” upgrade. *ACS EST Water* 1:1035–1046. <https://doi.org/10.1021/acsestwater.1c00010>
- Archer C, Andersen MB, Cloquet C, Conway TM, Dong S, Ellwood M, Moore R, Nelson J, Rehkämper M, Rouxel O, Samanta M, Shin K-C, Sohrin Y, Takano S, Wasylenki L (2017) Inter-calibration of a proposed new primary reference standard AA-ETH Zn for zinc isotopic analysis. *J Anal Spectrom* 32:415–419. <https://doi.org/10.1039/c6ja00282j>
- Balistrieri LS, Borrok DM, Wanty RB, Ridley WI (2008) Fractionation of Cu and Zn isotopes during adsorption onto amorphous Fe(III) oxyhydroxide: Experimental mixing of acid rock drainage and ambient river water. *Geochim Cosmochim Acta* 72:311–328. <https://doi.org/10.1016/j.gca.2007.11.013>
- Barletta M, Lima ARA, Costa MF (2019) Distribution, sources and consequences of nutrients, persistent organic pollutants, metals and microplastics in South American estuaries. *Sci Total Environ* 651:1199–1218. <https://doi.org/10.1016/j.scitotenv.2018.09.276>
- Bronk Ramsey C (2008) Deposition models for chronological records. *Quat Sci Rev* 27:42–60. <https://doi.org/10.1016/j.quascirev.2007.01.019>
- Bronk Ramsey C (2009) Bayesian analysis of radiocarbon dates. *Radiocarbon* 51:337–360. <https://doi.org/10.1017/s0033822200033865>
- Bronk Ramsey C, Lee S (2013) Recent and planned developments of the program OxCal. *Radiocarbon* 55:720–730. <https://doi.org/10.1017/S0033822200057878>
- Bryan AL, Dong S, Wilkes EB, Wasylenki LE (2015) Zinc isotope fractionation during adsorption onto Mn oxyhydroxide at low and high ionic strength. *Geochim Cosmochim Acta* 157:182–197. <https://doi.org/10.1016/j.gca.2015.01.026>
- Canavan RW, Van Cappellen P, Zwolsman JGG, van den Berg GA, Slomp CP (2007) Geochemistry of trace metals in a fresh water sediment: Field results and diagenetic modeling. *Sci Total Environ* 381:263–279. <https://doi.org/10.1016/j.scitotenv.2007.04.001>
- Chen CW, Kao CM, Chen CF, Dong CD (2007) Distribution and accumulation of heavy metals in the sediments of Kaohsiung Harbor, Taiwan. *Chemosphere* 66:1431–1440. <https://doi.org/10.1016/j.chemosphere.2006.09.030>
- Chen J, Gaillardet J, Louvat P (2008) Zinc isotopes in the Seine River waters, France: a probe of anthropogenic contamination. *Environ Sci Technol* 42:6494–6501. <https://doi.org/10.1021/es800725z>
- Chen H, Savage PS, Teng FZ, Helz RT, Moynier F (2013) Zinc isotope fractionation during magmatic differentiation and the isotopic composition of the bulk Earth. *Earth Planet Sci Lett* 369–370:34–42. <https://doi.org/10.1016/j.epsl.2013.02.037>

- Conway TM, Rosenberg AD, Adkins JF, John SG (2013) A new method for precise determination of iron, zinc and cadmium stable isotope ratios in seawater by double-spike mass spectrometry. *Anal Chim Acta* 793:44–52. <https://doi.org/10.1016/j.aca.2013.07.025>
- Cooke CA, Bindler R (2015) Lake sediment records of preindustrial metal pollution. In: Blais JM, Rosen MR, Smol JP (eds) *Environmental contaminants: using natural archives to track sources and long-term trends of pollution*. Springer, Dordrecht, pp 101–119
- Dang DH, Lenoble V, Durrieu G, Omanović D, Mullot JU, Mounier S, Garnier C (2015) Seasonal variations of coastal sedimentary trace metals cycling: insight on the effect of manganese and iron (oxy)hydroxides, sulphide and organic matter. *Mar Pollut Bull* 92:113–124. <https://doi.org/10.1016/j.marpolbul.2014.12.048>
- de Souza Machado AA, Spencer K, Kloas W, Toffolon M, Zarfl C (2016) Metal fate and effects in estuaries: a review and conceptual model for better understanding of toxicity. *Sci Total Environ* 541:268–281. <https://doi.org/10.1016/j.scitotenv.2015.09.045>
- Desautly AM, Petelet-Giraud E (2020) Zinc isotope composition as a tool for tracing sources and fate of metal contaminants in rivers. *Sci Total Environ* 728:138599. <https://doi.org/10.1016/j.scitotenv.2020.138599>
- Dong S, Wasylenki LE (2016) Zinc isotope fractionation during adsorption to calcite at high and low ionic strength. *Chem Geol* 447:70–78. <https://doi.org/10.1016/j.chemgeo.2016.10.031>
- Dong S, Ochoa Gonzalez R, Harrison RM, Green D, North R, Fowler G, Weiss D (2017) Isotopic signatures suggest important contributions from recycled gasoline, road dust and non-exhaust traffic sources for copper, zinc and lead in PM₁₀ in London, United Kingdom. *Atmos Environ* 165:88–98. <https://doi.org/10.1016/j.atmosenv.2017.06.020>
- Federation of Electro Plating Industry, Japan (2003) Members by prefecture. <https://zentoren.or.jp/en/zentoren/kumiai-support.html>. Assessed 26 May 2022
- Garrett RG, Reimann C, Hron K, Kynčlová P, Filzmoser P (2017) Finally, a correlation coefficient that tells the geochemical truth. *News Assoc Appl Geochem* 176:1–10
- Garrett RG (2018) Package “rgr.” *Appl Geochemistry* EDA
- Geological Survey of Japan, AIST (eds) (2015) *Seamless Digital Geological Map of Japan 1:200,000*, May 29, 2015 version. Geological Survey of Japan, National Institute of Advanced Industrial Science and Technology, Tsukuba, Japan
- Gioia S, Weiss D, Coles B, Arnold T, Babinski M (2008) Accurate and precise zinc isotope ratio measurements in urban aerosols. *Anal Chem* 80:9776–9780. <https://doi.org/10.1021/ac8019587>
- Heaton TJ, Köhler P, Butzin M, Bard E, Reimer RW, Austin WEN, Bronk Ramsey C, Grootes PM, Hughen KA, Kromer B, Reimer PJ, Adkins J, Burke A, Olsen CMS, Skinner LC (2020) Marine20: the marine radiocarbon age calibration curve (0–55,000 cal BP). *Radiocarbon* 62:779–820. <https://doi.org/10.1017/RDC.2020.68>
- Hoshika A, Shiozawa T, Matsumoto E (1983) Sedimentation rate and heavy metal pollution in sediments in Harima Nada (Harima Sound), Seto Inland Sea. *J Oceanogr Soc Jpn* 39:82–87. <https://doi.org/10.1007/BF02210762> (in Japanese)
- Hosono T, Su CC, Okamura K, Taniguchi M (2010) Historical record of heavy metal pollution deduced by lead isotope ratios in core sediments from the Osaka Bay, Japan. *J Geochem Explor* 107:1–8. <https://doi.org/10.1016/j.gexplo.2010.05.003>
- Inano S, Yamazaki H, Yoshikawa S (2004) The History of Heavy Metal Pollution during the Last 100 Years, Recorded in Sediment Cores from Osaka Castle Moat, Southwestern Japan. *Quat Res* 43:275–286. <https://doi.org/10.4116/jaqua.43.275> (in Japanese)
- Irizuki T, Hirose K, Ueda Y, Fujihara Y, Ishiga H, Seto K (2018) Ecological shifts due to anthropogenic activities in the coastal seas of the Seto Inland Sea, Japan, since the 20th century. *Mar Pollut Bull* 127:637–653. <https://doi.org/10.1016/j.marpolbul.2017.12.050>
- Irizuki T, Takahashi J, Seto K, Ishiga H, Fujihara Y, Kawano S (2022) Response of bay ostracod assemblages to Late Holocene sea-level, centennial-scale climate, and human-induced factors in northeast Beppu Bay. *Jpn Mar Micropaleontol* 174:102002. <https://doi.org/10.1016/j.marmicro.2021.102002>
- Itihara M, Yoshikawa S, Kamei T, Nasu T (1988) Stratigraphic Subdivision of Quaternary Deposits in Kinki District, Japan. *Mem Geol Soc Jpn* 30:111–125 (in Japanese)
- Jeong H, Ra K, Choi JY (2021) Copper, zinc and lead isotopic delta values and isotope ratios of various geological and biological reference materials. *Geostand Geonanal Res* 45:551–563. <https://doi.org/10.1111/ggr.12379>
- John SG, Genevieve Park J, Zhang Z, Boyle EA (2007) The isotopic composition of some common forms of anthropogenic zinc. *Chem Geol* 245:61–69. <https://doi.org/10.1016/j.chemgeo.2007.07.024>
- Juillot F, Maréchal C, Ponthieu M, Cacaly S, Morin G, Benedetti M, Hazemann JL, Proux O, Guyot F (2008) Zn isotopic fractionation caused by sorption on goethite and 2-Lines ferrihydrite. *Geochim Cosmochim Acta* 72:4886–4900. <https://doi.org/10.1016/j.gca.2008.07.007>
- Juillot F, Maréchal C, Morin G, Jouvin D, Cacaly S, Telouk P, Benedetti MF, Ildefonse P, Sutton S, Guyot F, Brown GE (2011) Contrasting isotopic signatures between anthropogenic and geogenic Zn and evidence for post-depositional fractionation processes in smelter-impacted soils from Northern France. *Geochim Cosmochim Acta* 75:2295–2308. <https://doi.org/10.1016/j.gca.2011.02.004>
- Kajiyama H, Itihara M (1986) *Osaka Heiya no Oitachi (Life History of the Osaka Plain)*. Aoki Shoten, Tokyo (in Japanese)
- Kajiyama H, Itihara M (1972) The developmental history of the Osaka Plain with references to the radio-carbon dates. *Geol Soc Jpn* 7:101–112 (in Japanese)
- Kavner A, John SG, Sass S, Boyle EA (2008) Redox-driven stable isotope fractionation in transition metals: application to Zn electroplating. *Geochim Cosmochim Acta* 72:1731–1741. <https://doi.org/10.1016/j.gca.2008.01.023>
- Kawahata H, Yamashita S, Yamaoka K, Okai T, Shimoda G, Ima N (2014) Heavy metal pollution in Ancient Nara, Japan, during the eighth century. *Prog Earth Planet Sci* 1:15. <https://doi.org/10.1186/2197-4284-1-15>
- Komárek M, Ratič G, Vaňková Z, Šípková A, Chrástný V (2022) Metal isotope complexation with environmentally relevant surfaces: opening the isotope fractionation black box. *Crit Rev Environ Sci Technol* 52:3573–3603. <https://doi.org/10.1080/10643389.2021.1955601>
- Kusaka M (2012) History from the topography. Kodansha, Tokyo (in Japanese)
- Kuwaie M, Yamamoto M, Ikehara K, Irino T, Takemura K, Sagawa T, Sakamoto T, Ikehara M, Takeoka H (2013) Stratigraphy and wiggle-matching-based age-depth model of late Holocene marine sediments in Beppu Bay, southwest Japan. *J Asian Earth Sci* 69:133–148. <https://doi.org/10.1016/j.jseaes.2012.07.002>
- Kynčlová P, Hron K, Filzmoser P (2017) Correlation between compositional parts based on symmetric balances. *Math Geosci* 49:777–796. <https://doi.org/10.1007/s11004-016-9669-3>
- Long ER, Macdonald DD, Smith SL, Calder FD (1995) Incidence of adverse biological effects within ranges of chemical concentrations in marine and estuarine sediments. *Environ Manage* 19:81–97. <https://doi.org/10.1007/BF02472006>
- Maréchal CN, Télouk P, Albarède F (1999) Precise analysis of copper and zinc isotopic compositions by plasma-source mass spectrometry. *Chem Geol* 156:251–273. [https://doi.org/10.1016/S0009-2541\(98\)00191-0](https://doi.org/10.1016/S0009-2541(98)00191-0)
- Matsuda J (2008) New perspectives in archaeology: Earth science at the archaeological sites (4) For reconstruction of landscape. *Q Archaeol Stud* 54:108–111 (in Japanese)
- Matsuzaki H, Nakano C, Yamashita H, Maejima Y, Miyairi Y, Wakasa S, Horiuchi K (2004) Current status and future direction of MALT, The University of Tokyo. *Nucl Instrum Methods Phys Res Sect B* 223–224:92–99. <https://doi.org/10.1016/j.nimb.2004.04.022>
- Mavromatis V, González AG, Dietzel M, Schott J (2019) Zinc isotope fractionation during the inorganic precipitation of calcite: towards a new pH proxy. *Geochim Cosmochim Acta* 244:99–112. <https://doi.org/10.1016/j.gca.2018.09.005>
- Nesbitt HW, Young GM (1982) Early proterozoic climates and plate motions inferred from major element chemistry of lutites. *Nature* 299:715–717. <https://doi.org/10.1038/299715a0>
- Nitzsche KN, Yoshimura T, Ishikawa NF, Ogawa NO, Suzuki K, Ohkouchi N (2021) Trace metal geochemical and Zn stable isotope data as tracers for anthropogenic metal contributions in a sediment core from Lake Biwa. *Jpn Appl Geochem* 134:105107. <https://doi.org/10.1016/j.japgeochem.2021.105107>
- Ochoa Gonzalez R, Weiss D (2015) Zinc isotope variability in three coal-fired power plants: a predictive model for determining isotopic fractionation during combustion. *Environ Sci Technol* 49:12560–12567. <https://doi.org/10.1021/acs.est.5b02402>

- Ochoa Gonzalez R, Strekopytov S, Amato F, Querol X, Weiss D (2016) New insights from zinc and copper isotopic compositions into the sources of atmospheric particulate matter from two major European cities. *Environ Sci Technol* 50:9816–9824. <https://doi.org/10.1021/acs.est.6b00863>
- Ogawa NO, Nagata T, Kitazato H, Ohkouchi N (2010) Ultra-sensitive elemental analyzer/isotope ratio mass spectrometer for stable nitrogen and carbon isotope analyses. In: Ohkouchi N, Tayasu I, Koba K (eds) *Earth, life, and isotopes*. Kyoto University Press, pp 339–353
- Pearson R (2016) *Osaka archaeology*. Archaeopress Publishing Ltd, Oxford
- Rauret G, López-Sánchez JF, Sahuquillo A, Rubio R, Davidson C, Ure A, Quevauviller P (1999) Improvement of the BCR three step sequential extraction procedure prior to the certification of new sediment and soil reference materials. *J Environ Monit* 1:57–61. <https://doi.org/10.1039/a807854h>
- Reimann C, Filzmoser P, Hron K, Kynčlová P, Garrett RG (2017) A new method for correlation analysis of compositional (environmental) data: a worked example. *Sci Total Environ* 607–608:965–971. <https://doi.org/10.1016/j.scitotenv.2017.06.063>
- Rhee SN, Aikens CM, Choi SR, Ro HJ (2007) Korean contributions to agriculture, technology, and state formation in Japan: archaeology and history of an epochal thousand years, 400 B.C.–A.D. 600. *Asian Perspect* 46:404–459. <https://doi.org/10.1353/asi.2007.0016>
- Rudnick RL, Gao S (2014) Composition of the continental crust. In: Holland HD, Turekian KK (eds) *Treatise on geochemistry*. Elsevier, pp 1–51. <https://doi.org/10.1016/B978-0-08-095975-7.00301-6>
- Sahuquillo A, López-Sánchez JF, Rubio R, Rauret G, Thomas RP, Davidson CM, Ure AM (1999) Use of a certified reference material for extractable trace metals to assess sources of uncertainty in the BCR three-stage sequential extraction procedure. *Anal Chim Acta* 382:317–327. [https://doi.org/10.1016/S0003-2670\(98\)00754-5](https://doi.org/10.1016/S0003-2670(98)00754-5)
- Saito O (2002) Edo and Osaka: an origin of modern Japanese cities. NTT Publishing, Tokyo (**in Japanese**)
- Sakata M, Okuizumi S, Mashio AS, Ohno T, Sakata S (2019) Evaluation of pollution sources of zinc in Tokyo Bay based on zinc isotope ratio in sediment core. *J Geosci Environ Prot* 7:141–154. <https://doi.org/10.4236/gep.2019.78010>
- Sivry Y, Riotte J, Sonke JE, Audry S, Schäfer J, Viers J, Blanc G, Freyrier R, Dupré B (2008) Zn isotopes as tracers of anthropogenic pollution from Zn-ore smelters The Riou Mort-Lot River system. *Chem Geol* 255:295–304. <https://doi.org/10.1016/j.chemgeo.2008.06.038>
- Smith CW, Fehrenbacher JS, Goldstein ST (2020) Incorporation of heavy metals in experimentally grown foraminifera from Sapelo Island, Georgia and Little Duck Key, Florida, U.S.A. *Mar Micropaleontol* 156:101854. <https://doi.org/10.1016/j.marmicro.2020.101854>
- Sossi PA, Halverson GP, Nebel O, Eggins SM (2015) Combined separation of Cu, Fe and Zn from rock matrices and improved analytical protocols for stable isotope determination. *Geostand Geoanal Res* 39:129–149. <https://doi.org/10.1111/j.1751-908X.2014.00298.x>
- Souto-Oliveira CE, Babinski M, Araújo DF, Andrade MF (2018) Multi-isotopic fingerprints (Pb, Zn, Cu) applied for urban aerosol source apportionment and discrimination. *Sci Total Environ* 626:1350–1366. <https://doi.org/10.1016/j.scitotenv.2018.01.192>
- Souto-Oliveira CE, Babinski M, Araújo DF, Weiss DJ, Ruiz IR (2019) Multi-isotope approach of Pb, Cu and Zn in urban aerosols and anthropogenic sources improves tracing of the atmospheric pollutant sources in megacities. *Atmos Environ* 198:427–437. <https://doi.org/10.1016/j.atmosenv.2018.11.007>
- Suzuki H, Matsuo N, Ito K, Kubo K, Sekiyama, H, Nagayama M, Goto S, Haga N, Imai N (1998) *Archaeological Reports of the Sumitomo copper refinery Site*. Osaka City Cultural Properties Association, Osaka (**in Japanese**)
- Takano S, Tsuchiya M, Imai S, Yamamoto Y, Fukami Y, Suzuki K, Sohrin Y (2021) Isotopic analysis of nickel, copper, and zinc in various freshwater samples for source identification. *Geochem J* 55:171–183. <https://doi.org/10.2343/geochemj.2.0627>
- Thapalia A, Borrok DM, Van Metre PC, Musgrove M, Landa ER (2010) Zn and Cu isotopes as tracers of anthropogenic contamination in a sediment core from an Urban Lake. *Environ Sci Technol* 44:1544–1550. <https://doi.org/10.1021/es902933y>
- Thapalia A, Borrok DM, Van Metre PC, Wilson J (2015) Zinc isotopic signatures in eight lake sediment cores from across the United States. *Environ Sci Technol* 49:132–140. <https://doi.org/10.1021/es5036893>
- Tonh  MS, Garnier J, Ara jo DF, Cunha BCA, Machado W, Dantas E, Ara jo R, Kutter VT, Bonnet MP, Seyler P (2020) Behavior of metallurgical zinc contamination in coastal environments: a survey of Zn from electroplating wastes and partitioning in sediments. *Sci Total Environ* 743:140610. <https://doi.org/10.1016/j.scitotenv.2020.140610>
- Yasuhara M, Yamazaki H (2005) The impact of 150 years of anthropogenic pollution on the shallow marine ostracode fauna, Osaka Bay, Japan. *Mar Micropaleontol* 55:63–74. <https://doi.org/10.1016/j.marmicro.2005.02.005>
- Yasuhara M, Irizuki T, Yoshikawa S, Nanayama F (2002) Holocene sea-level changes in Osaka Bay, western Japan: ostracode evidence in a drilling core from the southern Osaka Plain. *J Geol Soc Jpn* 108:633–643. https://doi.org/10.5575/geosoc.108.10_633
- Yasuhara M, Yamazaki H, Irizuki T, Yoshikawa S (2003) Temporal changes of ostracode assemblages and anthropogenic pollution during the last 100 years, in sediment cores from Hiroshima Bay, Japan. *Holocene* 13:527–536. <https://doi.org/10.1191/0959683603h1643rp>
- Yasuhara M, Yamazaki H, Tsujimoto A, Hirose K (2007) The effect of long-term spatiotemporal variations in urbanization-induced eutrophication on a benthic ecosystem, Osaka Bay, Japan. *Limnol Oceanogr* 52:1633–1644. <https://doi.org/10.4319/lo.2007.52.4.1633>
- Yokoyama T, Makishima A, Nakamura E (1999) Evaluation of the coprecipitation of incompatible trace elements with fluoride during silicate rock dissolution by acid digestion. *Chem Geol* 157:175–187. [https://doi.org/10.1016/S0009-2541\(98\)00206-X](https://doi.org/10.1016/S0009-2541(98)00206-X)
- Yokoyama Y, Miyairi Y, Matsuzaki H, Tsunomori F (2007) Relation between acid dissolution time in the vacuum test tube and time required for graphitization for AMS target preparation. *Nucl Instrum Methods Phys Res Sect B* 259:330–334. <https://doi.org/10.1016/j.nimb.2007.01.176>
- Yokoyama Y, Miyairi Y, Aze T, Yamane M, Sawada C, Ando Y, de Natris M, Hirabayashi S, Ishiwa T, Sato N, Fukuyo N (2019) A single stage accelerator mass spectrometry at the atmosphere and ocean research Institute, The University of Tokyo. *Nucl Instrum Methods Phys Res Sect B* 456:311–316. <https://doi.org/10.1016/j.nimb.2019.01.055>
- Young GM, Nesbitt HW (1998) Processes controlling the distribution of Ti and Al in weathering profiles, siliciclastic sediments and sedimentary rocks. *J Sedim Res* 68:448–455. <https://doi.org/10.2110/jsr.68.448>
- Zong Y, Yu F, Huang G, Lloyd JM, Yim WWS (2010) Sedimentary evidence of Late Holocene human activity in the Pearl River delta, China. *Earth Surf Process Landforms* 35:1095–1102. <https://doi.org/10.1002/esp.1970>

Publisher's Note

Springer Nature remains neutral with regard to jurisdictional claims in published maps and institutional affiliations.

Submit your manuscript to a SpringerOpen[®] journal and benefit from:

- Convenient online submission
- Rigorous peer review
- Open access: articles freely available online
- High visibility within the field
- Retaining the copyright to your article

Submit your next manuscript at ► [springeropen.com](https://www.springeropen.com)